Journal of Catalysis xxx (xxxx) xxx

Contents lists available at ScienceDirect

Journal of Catalysis

journal homepage: www.elsevier.com/locate/jcat

$Co_xFe_{1-x}Al_2O_{4+\delta}$ composite oxides supported Pt nanoparticles as efficient and recyclable catalysts for the liquid-phase selective hydrogenation of cinnamaldehyde

Huiyue Xin, Yujie Xue, Wenbo Zhang, Peng Wu, Xiaohong Li *

Shanghai Key Laboratory of Green Chemistry and Chemical Processes, School of Chemistry and Molecular Engineering, East China Normal University, 3663 North Zhongshan Rd., Shanghai 200062, China

ARTICLE INFO

Article history:
Received 29 July 2019
Revised 11 September 2019
Accepted 29 September 2019
Available online xxxx

Keywords:
$Co_xFe_{1-x}Al_2O_{4+\delta}$ composite oxides
Pt catalyst
Selective hydrogenation
Cinnamaldehyde
Cinnamyl alcohol

ABSTRACT

$Co_xFe_{1-x}Al_2O_{4+\delta}$ composite oxides were prepared using a sol-gel method with glucose as hard template. Pt nanoparticles supported on $Co_xFe_{1-x}Al_2O_{4+\delta}$ were employed for the liquid-phase selective hydrogenation of cinnamaldehyde (CAL) to yield the desired cinnamyl alcohol (COL). The activity increased with the x value; while the selectivity to COL almost kept above 90% despite of different x values. Upon investigation of kinetic behaviour with $Pt/Co_{0.5}Fe_{0.5}Al_2O_{4+\delta}$ as a model catalyst, the initial activity (in terms of TOF, defined as the converted CAL molecules per surface Pt atoms per second) of 4.1 s^{-1} was furnished. As for the selectivity to COL, it almost kept around 95% at whatever CAL conversions despite of the reaction temperatures. $Pt/Co_{0.5}Fe_{0.5}Al_2O_{4+\delta}$ catalyst can also be recycled for at least 10 times without obvious loss in activity or selectivity toward COL. This suggests that the active sites on the $Pt/Co_{0.5}Fe_{0.5}Al_2O_{4+\delta}$ catalyst preferentially adsorb and activate CAL via the terminal carbonyl groups. XPS analyses, H_2-TPR, and CO-IR studies reveal that the intimate contact of Pt nanoparticles with FeO_x or CoO_x plays an important role in determining the catalytic performance of the $Pt/Co_xFe_{1-x}Al_2O_{4+\delta}$ catalysts. The Pt $^{\delta+}/Pt^0$ ratio increased with the x value so that the $Pt/CoAl_2O_4$ was the most active among the $Pt/Co_xFe_{1-x}Al_2O_{4+\delta}$ catalysts.

1. Introduction

Cinnamaldehyde (CAL), one of typical α,β-unsaturated aldehydes, can be selectively hydrogenated to corresponding α,β-unsaturated alcohol, cinnamyl alcohol (COL). COL is the valuable intermediate and can be widely used in perfumes, pharmaceuticals, pesticides, foods, etc [1]. However, the selective hydrogenation of C═O double bond in CAL to yield COL is not thermodynamically favorable due to the conjugate effect between C═C double bond and C═O double bond. Nevertheless, great efforts have been made to develop efficient catalysts with attractive chemoselectivity in recent two decades [2–8].

After literature survey, it can be found that Pt-based catalysts are widely investigated for the selective hydrogenation of CAL to yield COL. However, traditional Pt catalysts can only show mediocre selectivity toward COL in most cases (Scheme 1B) [9,10]. To improve the catalytic performance, particularly the COL selectivity at higher CAL conversions with the Pt-based catalysts, many studies have been focused on the issues as follows: (1) support-induced modification of Pt electronic properties using special materials as support materials, such as CeO_2-ZrO_2 [11], SiO_2-Al_2O_3 [12], TiO_2-SiO_2 [13], CoAl mixed metal oxide nanosheets [14], $YCo_xFe_{1-x}O_3$ perovskite composites [15] and FeFe-LDH [16]; (2) control of the Pt morphologies including controllable construction of 1D metal nanowires or control of the exposure of special Pt facets [17–19]; (3) adopting the second metal component like Fe [9,10], Co [20] and Sn [21] to modulate the electronic properties of Pt nanoparticles; (4) confinement of Pt nanoparticles within metal-organic frameworks [22,23] or surface modification of Pt catalysts by long-chain ligands or thiols [24–26]. In some cases, two or more strategies were adopted to achieve better results for the Pt-based catalysts, including activity and selectivity toward COL. According to the literature, the second metal such as Fe or Co is usually doped to improve the Pt-based catalysts via modulating the Pt surface electronic properties. However, when used as additives, Fe, Co or other second metals usually exist as their oxide aggregates, so that the interaction of Pt with the second metal oxides is difficult to control owing to lack of intimate contact if they are not highly and uniformly dispersed.

Spinel composite metal oxides (SCMOs), with an adjustable degeneration and structural stability, are widely used as redox

---

* Corresponding author.
E-mail address: xhli@chem.ecnu.edu.cn (X. Li).

https://doi.org/10.1016/j.jcat.2019.09.042

Please cite this article as: H. Xin, Y. Xue, W. Zhang et al., $Co_xFe_{1-x}Al_2O_{4+\delta}$ composite oxides supported Pt nanoparticles as efficient and recyclable catalysts for the liquid-phase selective hydrogenation of cinnamaldehyde, Journal of Catalysis, https://doi.org/10.1016/j.jcat.2019.09.042

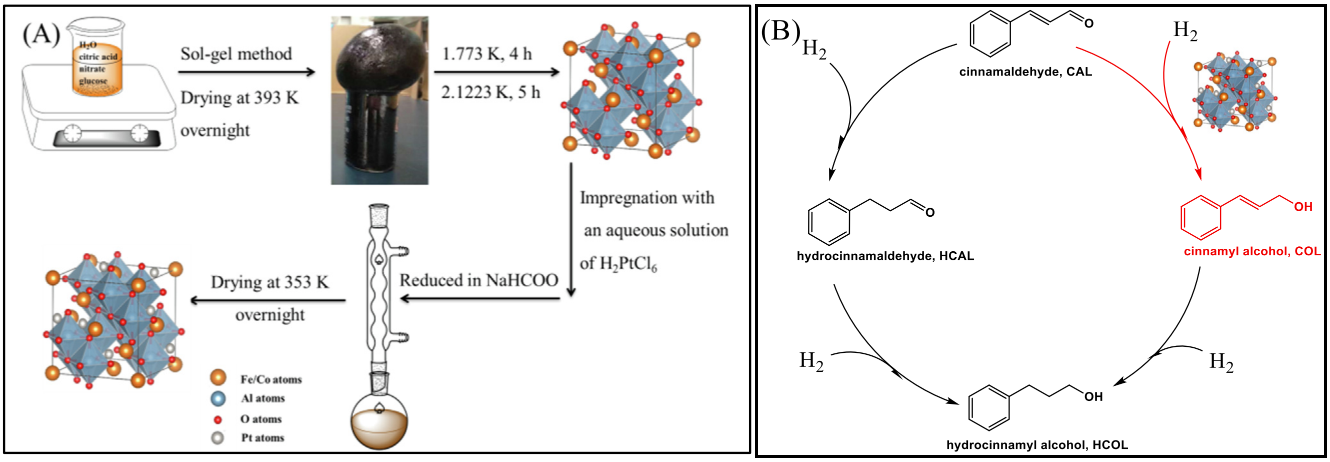

Scheme 1. (A) Design and preparation of the Pt catalyst supported on $Co_xFe_{1-x}Al_2O_{4+\delta}$ SCMOs and (B) the selective hydrogenation of CAL to the desired COL.

catalysts and catalyst supports [27–30]. Monoclinic AB_2O_4 SCMOs (where A = Mg, Fe, Co, Ni, Zn, or Mn; B = Al, Cr, Ga, Co, or Fe), have attracted considerable attention because of their versatile physicochemical properties. We notice that Fe or Co can serve as "A" site ions, while Al can serve as "B" site ions in AB_2O_4 SCMOs, respectively. Therefore, both Fe/Co and Al can be well isolated and dispersed uniformly, although they still exist in their oxides. Under this circumstances, there will be intimate contact between Pt nanoparticles and FeO_x/CoO_x or AlO_x when $Fe(Co)Al_2O_{4+\delta}$ SCMOs are used to load Pt nanoparticles. Therefore, the interaction between Pt nanoparticles and FeO_x/CoO_x or AlO_x becomes possible and controllable.

Considering that Fe/Co are better additives for the Pt-based catalysts towards the selective hydrogenation of CAL to yield COL and that alumina is a common support material for Pt nanoparticles, we are eager to prepare $Co_xFe_{1-x}Al_2O_{4+\delta}$ SCMOs (x represents the Co/(Co + Fe) molar ratio, $x = 0–1$) for Pt nanoparticles towards the selective hydrogenation of CAL to yield COL. Nevertheless, SCMOs prepared by a traditional co-precipitation method usually suffer from a drawback of extremely low specific surface area, which greatly limits the application in catalysis. Therefore, preparation of SCMOs with relatively larger specific surface area becomes a challenge. Hard template method provides an efficient way to prepare the porous SCMOs with comparatively larger specific surface area. Herein, we prepared $Co_xFe_{1-x}Al_2O_{4+\delta}$ SCMOs with a modified sol-gel method using glucose as template, and then investigated their catalytic performance after loading Pt nanoparticles for the selective liquid-phase hydrogenation of CAL. The $Co_xFe_{1-x}Al_2O_{4+\delta}$ SCMOs have a relatively larger specific surface area when compared with those obtained via the traditional co-precipitation method. The Co/(Fe + Co) molar ratio, Pt-FeO_x/CoO_x interaction and the surface electronic properties of Pt/$Co_xFe_{1-x}Al_2O_{4+\delta}$ catalysts were investigated in detail. As a result, the Pt/$Co_{0.5}Fe_{0.5}Al_2O_{4+\delta}$ catalyst furnished an initial activity (in terms of TOF, defined as the converted CAL molecules per surface Pt atoms per second) of 4.1 s^{-1} along with 95% selectivity toward COL under mild conditions.

2. Experimental

2.1. Chemicals

Chloroplatinic acid hexahydrate ($H_2PtCl_6{\cdot}6H_2O$) and other chemicals were of analytical grade and used as received. CAL was purchased from Alfa Aesar and used as received. Other reagents including $Fe(NO_3)_3{\cdot}9H_2O$, $Al(NO_3)_3{\cdot}9H_2O$, $Co(NO_3)_2{\cdot}6H_2O$, citric acid, glucose, and isopropanol were purchased from Sinopharm Chemical Reagent Co., Ltd. and used as received.

2.2. Preparation of $Co_xFe_{1-x}Al_2O_{4+\delta}$ SCMOs and related Pt catalysts

$Co_xFe_{1-x}Al_2O_{4+\delta}$ SCMOs were prepared by a modified sol-gel method. Taking the preparation of $Co_{0.5}Fe_{0.5}Al_2O_{4+\delta}$ SCMOs as an example, the detailed preparation procedures are as follows: a solution containing 0.003 M $Al(NO_3)_3{\cdot}9H_2O$, 0.0015 M $Co(NO_3)_2{\cdot}6H_2O$, and 0.0015 M $Fe(NO_3)_3{\cdot}9H_2O$ was mixed. Then, citric acid was added to the above solution to control the final citrate/transition metal ratio of 1/1. Subsequently, 5.0 M glucose aqueous solution was added to the above solution and stirred at RT for 3–4 h, followed by further stirring at 363 K till the sticky gel was formed. After that, the gel was dried at 393 K overnight. After grinding, the precursors were calcined in air at 773 K for 4 h, and then at 1223 K for additional 5 h to obtain the resultant $Co_{0.5}Fe_{0.5}Al_2O_{4+\delta}$ SCMOs. The $Co_xFe_{1-x}Al_2O_{4+\delta}$ SCMOs with other Co/(Fe + Co) molar ratios were prepared using the similar method as well. Because twice the amount of Co + Fe was adopted for the proposed $Co_xFe_{1-x}Al_2O_{4+\delta}$ composition, so there are redundant non-structural FeOx or CoOx simple oxides embedded in the $Co_xFe_{1-x}Al_2O_{4+\delta}$ SCMOs. In order to make sense and simplify the support designation, the SCMOs were denoted as $Co_xFe_{1-x}Al_2O_{4+\delta}$.

Nominal 5 wt% Pt/$Co_xFe_{1-x}Al_2O_{4+\delta}$ catalysts were prepared via an impregnation method using an aqueous solution of H_2PtCl_6 as Pt precursor. The suspension was stirred at RT for 4–6 h and then evaporated to remove the excess solvent, followed by drying at 353 K overnight. Then, the catalyst precursors were calcined in static air at 473 K for 2 h before reduction in an aqueous solution of sodium formate at 363 K for 2 h (Scheme 1A).

2.3. Catalyst characterization

The powder X-ray diffraction (XRD) patterns of the samples were collected on a Bruker D8 ADVANCE instrument using Cu Kα radiation (λ = 1.54178 Å) as X-ray source. Jade 6.0 software was used to match the crystalline phase of the materials with standard PDF cards. The N_2-physisorption of the samples were measured at 77 K on a Quantachrome Autosorb-3B system after the samples were evacuated at 473 K for 2 h. The Brunauer-Emmett-Teller (BET) specific surface area was calculated using the adsorption data in the relative pressure range from 0.05 to 0.35. The transmission electron microscopy (TEM) images were taken on an FEI Tecnai G2-TF30 microscope at an acceleration voltage of 300 kV. The

Please cite this article as: H. Xin, Y. Xue, W. Zhang et al., $Co_xFe_{1-x}Al_2O_{4+\delta}$ composite oxides supported Pt nanoparticles as efficient and recyclable catalysts for the liquid-phase selective hydrogenation of cinnamaldehyde, Journal of Catalysis, https://doi.org/10.1016/j.jcat.2019.09.042

scanning electron microscopy (SEM) was performed using a Hitachi S-4800 microscope. The actual Pt loading of the samples were determined by Thermo Elemental IRIS Intrepid II XSP inductively coupled plasma-atomic emission spectroscopy (ICP-AES).

Temperature-programmed reduction of hydrogen (H_2-TPR) was conducted with a Micromeritics AutoChem II Chemisorption Analyzer. Prior to H_2-TPR experiments, the samples were pretreated in flowing Ar at 423 K for 0.5 h and then cooled to RT in flowing Ar (99.999%, 30 $mL\cdot min^{-1}$). After that, the sample was heated from RT to 1073 K with a ramp of 10 $K\cdot min^{-1}$ under a mixture of 10% H_2-Ar (30 $mL \cdot min^{-1}$). The rate of H_2 consumption was monitored by a gas chromatograph (GC) with a thermal conductivity detector (TCD).

Temperature-programmed desorption of hydrogen (H_2-TPD) was also carried out on Micromeritics AutoChem II Chemisorption Analyzer. The samples were pretreated at 473 K for 2 h under 10% H_2-Ar atmosphere and then cooled down to 323 K under flowing He atmosphere. After H_2 adsorption in 10% H_2-Ar mixture (50 $mL \cdot min^{-1}$) at 323 K for 1 h, the samples were purged with He for 2 h to remove the physically adsorbed species. The H_2 desorption was then conducted under He atmosphere with a temperature ramp of 10 $K\cdot min^{-1}$ from 323 to 1073 K.

Temperature programmed desorption of ammonia (NH_3-TPD) was also performed on Micromeritics AutoChem II Chemisorption Analyzer to characterize the acidity of the samples. The samples were firstly outgassed in flowing He (50 $mL\cdot min^{-1}$) at 673 K for 1 h, and then adsorption of ammonia was performed in a 10% NH_3-He (50 $mL\cdot min^{-1}$) at 323 K for 0.5 h. After removal of the physisorbed NH_3 by flowing He (50 $mL\cdot min^{-1}$), the chemisorbed NH_3 was analyzed with a TCD detector by heating from RT to 873 K at a ramp rate of 10 $K\cdot min^{-1}$ and then maintained at 873 K for 0.5 h under the flowing He.

The FT-IR spectra was measured to confirm the structure of $Co_xFe_{1-x}Al_2O_{4+\delta}$ SCMOs using a Nexus 870 FT-IR spectrometer in the range of 400–4000 cm^{-1} at a spectral resolution of 4 cm^{-1} and 32 scans. The sample powders were mixed with KBr (1 wt%) and pressed into self-supported disks at RT. The FT-IR spectra of the samples using CO as probe molecules were measured with Nicolet iS50 FT-IR spectrometer in transmission-absorption mode. The samples were pressed into self-supported wafers and put into the IR cell. Prior to CO adsorption, the samples were *in situ* pretreated under H_2 atmosphere at 473 K for 2 h and then cooled down to 308 K for CO adsorption. The IR spectra of the chemisorbed CO was recorded after physically adsorbed CO was evacuated. All of the FT-IR spectra were collected using 32 scans at a resolution of 4 cm^{-1}.

The X-ray photoelectron spectra (XPS) of the samples were measured with a Thermo Fisher Scientific ESCALAB 250Xi spectrometer with Al Kα radiation (1486.6 eV) as incident beam with a monochromator. The samples were *in situ* pre-treated in flowing hydrogen at 473 K for 2 h in a reactor attachment of the XPS spectrometer for comparison. The binding energy (BE) was calibrated using C-C binding energy at 284.6 eV in order to compare the BE with data in the literature. The spectra shown in the figures have been corrected by subtraction of a Shirley background. Spectral fitting and peak integration were done using the XPS PEAK software.

2.4. Catalytic test

The catalysts were tested for the liquid-phase selective hydrogenation of CAL in a 100 mL autoclave. For a typical test, 25 mg of Pt catalyst was pretreated in a specially designed quartz tube under H_2 (99.999% purity, 30 $mL\cdot min^{-1}$) at 473 K for 2 h before use. Then, the pretreated catalyst was immediately transferred into the autoclave without exposure to air and mixed with CAL and solvent (containing isopropanol and water with a volume ratio of 9:1). The reaction began when hydrogen (2.0 MPa, 99.999% purity) was introduced with stirring (1200 rpm) at 363 K. The reaction was stopped after a proper time and the products were analyzed using a GC (GC-2014, Shimadzu) equipped with a flame ionization detector (FID) and a capillary column (DM-WAX, 30 m × 0.32 mm × 0.25μm). The response factor of each component was calculated using standard samples and was used to calculate the conversion and selectivity.

It should be pointed out that the absence of internal and external mass transfer limitation in the reaction was verified by Weisz-Prater criterion and Mears criterion, respectively. The absence of heat transfer limitation in the reaction was verified by a Mears criterion [31,32]. At the maximum reaction rate, the $C_{WP} = 8.09 \times 10^{-6} < 1$ and the $C_M = 0.0633 < 0.15$, which assured the absence of mass transfer limitation. Mears criterion for external (interphase) heat transfer gave $\left|\frac{-\Delta H_r(-r'_A)\rho_b RE}{h_t T_b^2 R_g}\right| < 0.15$, demonstrating no heat transfer limitations (see the Support Information for the details). Moreover, we also made the Madon-Boudart test to confirm that conditions of strict kinetic control were maintained in this case (see Fig. S1 in the Supporting Information for the details) [33].

For the recycling reactions, the catalyst was recovered by centrifugation, washed with isopropanol for several times to remove the residual substrate and product after each run and then submitted to the next run with fresh solvent and reactant.

3. Results and discussion

3.1. General characterization of the supports and related Pt catalysts

The $Co_xFe_{1-x}Al_2O_{4+\delta}$ SCMOs were synthesized via a modified sol-gel method using glucose as template. The structure of the $Co_xFe_{1-x}Al_2O_{4+\delta}$ SCMOs was first characterized using XRD. As shown in Fig. 1A, $FeAl_2O_{4+\delta}$ and $Co_{0.3}Fe_{0.7}Al_2O_{4+\delta}$ composites exhibited too complicated diffraction patterns to assign simply (see Fig. S2 in the Supporting Information). With increase of Co amount, $Co_{0.5}Fe_{0.5}Al_2O_{4+\delta}$ and $Co_{0.7}Fe_{0.3}Al_2O_{4+\delta}$ displayed six representative sharp diffraction patterns at 2θ of 31.0°, 36.5°, 44.4°, 55.1°, 58.8° and 64.6°, respectively, which match well with the PDF card of $FeAl_2O_4$. Nonetheless, highly dispersed CoO simple oxides may also exist although they cannot be detected due to high and uniform dispersion (see Fig. S3 in the Supporting Information). If *x* value further increased to 1, $CoAl_2O_4$ also showed six sharp diffraction patterns at 2θ of 31.2°, 36.7°, 44.7°, 55.5°, 59.2°, and 65.0°, which can be ascribed to $CoAl_2O_4$ (2 2 0), (3 1 1), (4 0 0), (4 2 2), (5 1 1) and (4 4 0) planes, respectively (see Fig. S4 in the Supporting Information). When compared with those of $Co_{0.5}Fe_{0.5}Al_2O_{4+\delta}$ and $Co_{0.7}Fe_{0.3}Al_2O_{4+\delta}$, there is a little shift to higher angles for the diffraction angle of $CoAl_2O_4$. In addition, besides the $Co_xFe_{1-x}Al_2O_{4+\delta}$ composition presented in the catalyst, we cannot exclude the existence of simple oxides such as CoO, FeO, Fe_2O_3 because twice the amount of Co + Fe was adopted for the proposed $Co_xFe_{1-x}Al_2O_{4+\delta}$ composition. In order to verify the structure of $Co_xFe_{1-x}Al_2O_{4+\delta}$ SCMOs, FT-IR spectroscopy was adopted (Fig. 1B). For $CoAl_2O_4$, the spinel structure can be identified by two sharp bands at 685 and 559 cm^{-1}, which can be attributed to Al-O vibrations related to tetrahedral AlO_4 and octahedral AlO_6 groups in $CoAl_2O_4$ [34]. With decreasing *x* value while increasing the Fe amount in $Co_xFe_{1-x}Al_2O_{4+\delta}$ SCMOs, those two IR bands red-shifted obviously, which might be caused by impure phase. That is, doping of Fe in $Co_xFe_{1-x}Al_2O_{4+\delta}$ SCMOs changed the crystal structure clearly. This is in good agreement with the XRD results.

The relevant Pt catalysts were also characterized using XRD. As also displayed in Fig. 1A, the Pt/$Co_xFe_{1-x}Al_2O_{4+\delta}$ catalysts displayed the similar diffraction patterns to their supports, demonstrating

Please cite this article as: H. Xin, Y. Xue, W. Zhang et al., $Co_xFe_{1-x}Al_2O_{4+\delta}$ composite oxides supported Pt nanoparticles as efficient and recyclable catalysts for the liquid-phase selective hydrogenation of cinnamaldehyde, Journal of Catalysis, https://doi.org/10.1016/j.jcat.2019.09.042

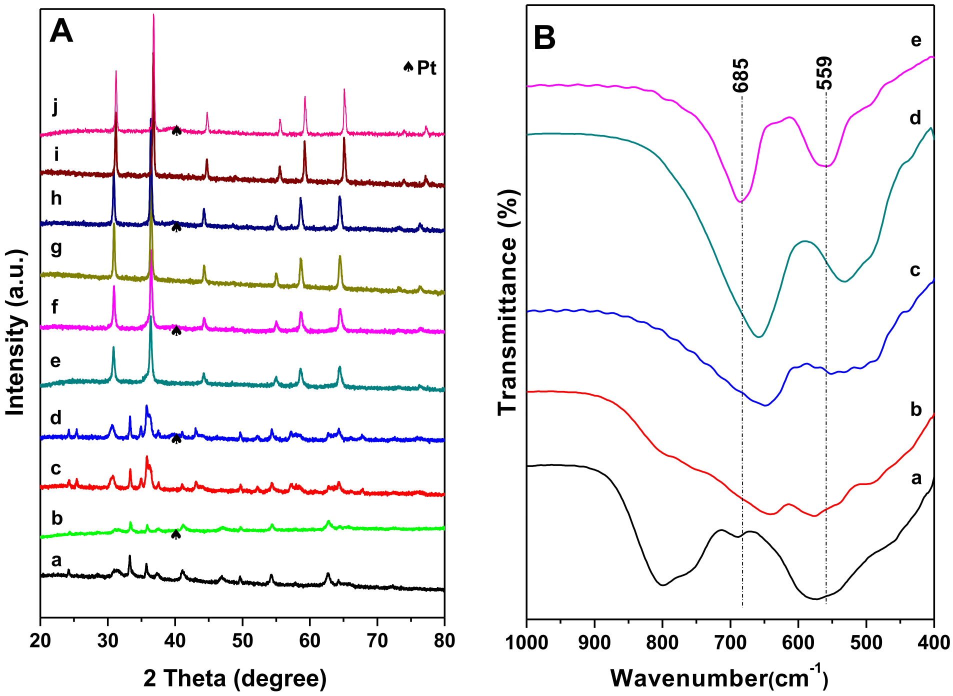

Fig. 1. (A) XRD patterns of (a) $FeAl_2O_{4+\delta}$, (b) $Pt/FeAl_2O_{4+\delta}$, (c) $Co_{0.3}Fe_{0.7}Al_2O_{4+\delta}$, (d) $Pt/Co_{0.3}Fe_{0.7}Al_2O_{4+\delta}$, (e) $Co_{0.5}Fe_{0.5}Al_2O_{4+\delta}$, (f) $Pt/Co_{0.5}Fe_{0.5}Al_2O_{4+\delta}$, (g) $Co_{0.7}Fe_{0.3}Al_2O_{4+\delta}$, (h) $Pt/Co_{0.7}Fe_{0.3}Al_2O_{4+\delta}$, (i) $CoAl_2O_4$ and (j) $Pt/CoAl_2O_4$; (B) FT-IR spectra of (a) $FeAl_2O_{4+\delta}$, (b) $Co_{0.3}Fe_{0.7}Al_2O_{4+\delta}$, (c) $Co_{0.5}Fe_{0.5}Al_2O_{4+\delta}$, (d) $Co_{0.7}Fe_{0.3}Al_2O_{4+\delta}$ and (e) $CoAl_2O_4$.

that loading of Pt nanoparticles did not destroy the structure of the $Co_xFe_{1-x}Al_2O_{4+\delta}$ SCMOs. Moreover, the diffraction patterns attributed to Pt(1 1 1) planes are extremely weak despite of different Co/(Co + Fe) molar ratios for the $Co_xFe_{1-x}Al_2O_{4+\delta}$ SCMOs, which can be a hint of high dispersion of Pt nanoparticles on $Co_xFe_{1-x}Al_2O_{4+\delta}$ surface. In addition, a part of Pt might be also in oxidized state that did not show intense metallic peaks.

The texture structures of $Co_xFe_{1-x}Al_2O_{4+\delta}$ SCMOs are critically important when they are used as supports. Therefore, $Co_xFe_{1-x}Al_2O_{4+\delta}$ SCMOs were characterized by nitrogen sorption to get the information about the specific surface area, pore volume and pore size distribution. All $Co_xFe_{1-x}Al_2O_{4+\delta}$ SCMOs showed typical type I isotherms with an insignificant H_3-type hysteresis loop in the region of relative pressure 0.8–1.0, which is associated with capillary condensation in mesopores (Fig. 2A). All $Co_xFe_{1-x}Al_2O_{4+\delta}$ SCMOs have a BET specific surface area of 10.7–22.2 $m^2\cdot g^{-1}$ and a pore volume of 0.03–0.08 $cm^3\cdot g^{-1}$. For comparison, the $Co_{0.5}Fe_{0.5}Al_2O_{4+\delta}$ analogue was also prepared without using glucose as template, only having a BET specific surface area of 3.6 $m^2\cdot g^{-1}$ with a pore volume of 0.01 $cm^3\cdot g^{-1}$, which are much lower than those obtained with its analogue prepared using glucose as template. This confirms that preparation of $Co_xFe_{1-x}Al_2O_{4+\delta}$ SCMOs via a sol-gel method using glucose as template can indeed give rise to comparatively higher specific surface area and higher pore volume. After loading Pt nanoparticles, the BET specific surface areas of all Pt catalysts increased slightly in contrast with those of the supports, but the total pore volumes of all Pt catalysts remained almost the same. For clarity, the physicochemical parameters for all the samples are listed in Table 1. Elemental analysis results for $Pt/Co_xFe_{1-x}Al_2O_{4+\delta}$ catalysts based on ICP-AES characterization are also added in Table 1. The real Pt loadings for all the $Pt/Co_xFe_{1-x}Al_2O_{4+\delta}$ catalysts are in the range of 3.6–4.6 wt%, a little lower than

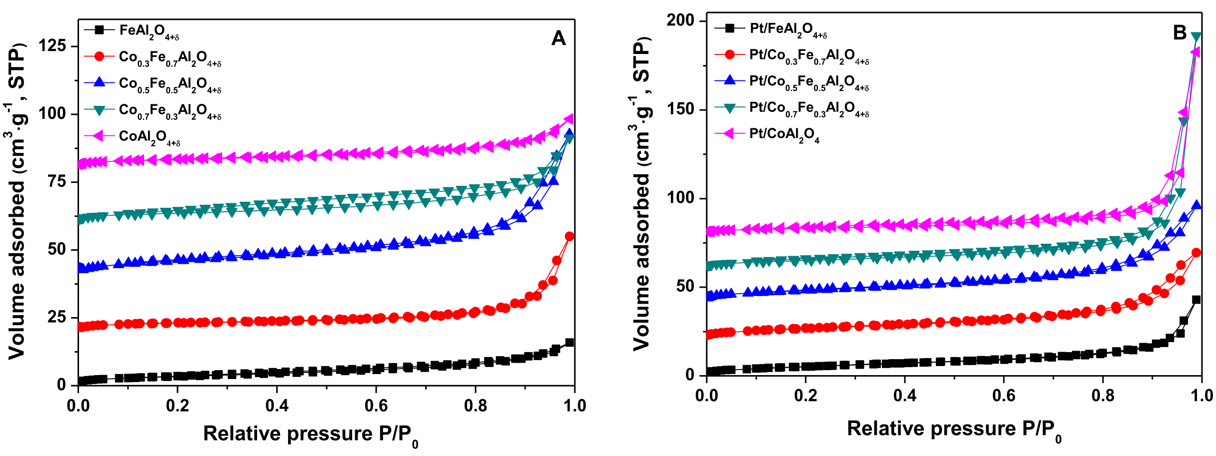

Fig. 2. N_2-physisorption isotherms of (A) $Co_xFe_{1-x}Al_2O_{4+\delta}$ SCMOs and (B) $Pt/Co_xFe_{1-x}Al_2O_{4+\delta}$ catalysts. The isotherms of $Co_{0.3}Fe_{0.7}Al_2O_{4+\delta}$, $Co_{0.5}Fe_{0.5}Al_2O_{4+\delta}$, $Co_{0.7}Fe_{0.3}Al_2O_{4+\delta}$ and $CoAl_2O_4$ were vertically translated by 20, 40, 60 and 80, respectively.

Please cite this article as: H. Xin, Y. Xue, W. Zhang et al., $Co_xFe_{1-x}Al_2O_{4+\delta}$ composite oxides supported Pt nanoparticles as efficient and recyclable catalysts for the liquid-phase selective hydrogenation of cinnamaldehyde, Journal of Catalysis, https://doi.org/10.1016/j.jcat.2019.09.042

Table 1
Physicochemical properties of $Co_xFe_{1-x}Al_2O_{4+\delta}$ supported Pt catalysts.

Catalyst	S_{BET}[a] ($m^2 \cdot g^{-1}$)	V_p[a] ($cm^3 \cdot g^{-1}$)	Pt particle size [b] (nm)	Disp.[c] (%)	Pt [d] (wt%)	Al [d] (wt%)	Co [d] (wt%)	Fe [d] (wt%)
$FeAl_2O_{4+\delta}$	12.2	0.06	–	–	–	–	–	–
$Co_{0.3}Fe_{0.7}Al_2O_{4+\delta}$	10.7	0.06	–	–	–	–	–	–
$Co_{0.5}Fe_{0.5}Al_2O_{4+\delta}$	22.2	0.08	–	–	–	–	–	–
$Co_{0.7}Fe_{0.3}Al_2O_{4+\delta}$	12.8	0.05	–	–	–	–	–	–
$CoAl_2O_4$	11.5	0.03	–	–	–	–	–	–
$Co_{0.5}Fe_{0.5}Al_2O_{4+\delta}$	3.6	0.01	–	–	–	–	–	–
$Pt/FeAl_2O_{4+\delta}$	20.4	0.06	2.2	51.4	3.8	14.8	–	31.9
$Pt/Co_{0.3}Fe_{0.7}Al_2O_{4+\delta}$	24.4	0.08	2.4	47.1	4.6	9.5	11.5	25.4
$Pt/Co_{0.5}Fe_{0.5}Al_2O_{4+\delta}$	29.3	0.08	3.4	33.2	3.6	15.1	15.0	16.7
$Pt/Co_{0.7}Fe_{0.3}Al_2O_{4+\delta}$	18.9	0.06	2.7	41.9	3.8	15.2	22.9	7.9
$Pt/CoAl_2O_4$	11.8	0.02	3.3	34.2	4.1	14.4	31.6	–

[a] The BET specific surface area and pore volume were calculated per g of sample.
[b] Pt particle size was calculated according to TEM characterizations.
[c] Dispersion was calculated according to D (%) × d (Pt particle size in nm) = 1.13.
[d] Determined by ICP-AES.

the nominal 5 wt%, because the Pt catalyst precursors were reduced in an aqueous solution of sodium formate at a reflux temperature, where some of Pt precursors were washed off from the support surface.

The morphology of the $Pt/Co_xFe_{1-x}Al_2O_{4+\delta}$ catalysts was characterized by SEM (Fig. 3). $Pt/FeAl_2O_{4+\delta}$ and $Pt/CoAl_2O_4$ displayed a coral-like morphology with an average size of about 100 nm; while for $Pt/Co_xFe_{1-x}Al_2O_{4+\delta}$ ($0 < x < 1$), a morphology with irregular particles was observed and the average particle size was increased to about 100–200 nm.

Some representative $Pt/Co_xFe_{1-x}Al_2O_{4+\delta}$ catalysts were also characterized using TEM (Fig. 4). Small and uniformly distributed Pt particles were observed for $Pt/Co_xFe_{1-x}Al_2O_{4+\delta}$, with Pt particle sizes ranging within 2.0–4.0 nm, which is consistent with the XRD results. The $Pt/FeAl_2O_{4+\delta}$ catalyst had an average size of 2.2 nm. It is clear that addition of Co with a small content ($x = 0.3$) in the $Pt/Co_{0.3}Fe_{0.7}Al_2O_{4+\delta}$ catalyst led to slightly larger Pt particle size, which was centered at 2.4 nm. With further increase of Co amount, Pt particle size gradually increased. As a result, the average Pt particle size was 3.3 nm for $Pt/CoAl_2O_4$. Furthermore, HRTEM images were also taken for some representative samples. For instance, (2 2 0) facets with the d-space of 0.286 nm was detected for $CoAl_2O_4$ support with the spinel structure (Fig. 4g). Moreover, Pt(1 1 1) facets with the d-space of 0.226 nm were detected for $Pt/FeAl_2O_{4+\delta}$ (Fig. 4h).

3.2. The selective hydrogenation of CAL over the $Pt/Co_xFe_{1-x}Al_2O_{4+\delta}$ catalysts

Firstly, the $Pt/Co_xFe_{1-x}Al_2O_{4+\delta}$ catalysts were applied to the liquid-phase selective hydrogenation of CAL. Table 2 lists the detailed results obtained with different $Pt/Co_xFe_{1-x}Al_2O_{4+\delta}$ catalysts. In a control experiment, the $Co_{0.5}Fe_{0.5}Al_2O_{4+\delta}$ SCMOs without loading Pt nanoparticles were adopted for the selective hydrogenation of CAL. As a result, the $Co_{0.5}Fe_{0.5}Al_2O_{4+\delta}$ SCMOs alone did not work at all within 30 min (Table 2, entry 1). This demonstrates that the $Co_xFe_{1-x}Al_2O_{4+\delta}$ SCMOs are not active without Pt nanoparticles for the tested reaction. After Pt nanoparticles were loaded, the $Pt/FeAl_2O_{4+\delta}$ catalyst gave about 78.6% CAL conversion and 90.8% selectivity toward COL within 30 min (Table 2, entry 2). When adding Co in SCMOs, the $Pt/Co_{0.3}Fe_{0.7}Al_2O_{4+\delta}$ catalyst showed a comparatively higher CAL conversion of 90.3%, in accompany with 94.3% COL selectivity (Table 2, entry 3). With further increase of Co amount in SCMOs, the $Pt/Co_{0.5}Fe_{0.5}Al_2O_{4+\delta}$ catalyst furnished excellent results including 94.2% CAL conversion and 95.0% COL selectivity under the same conditions (Table 2, entry 4). If the Co/(Fe + Co) molar ratio was further increased, the $Pt/Co_{0.7}Fe_{0.3}Al_2O_{4+\delta}$ catalyst was a little more efficient, furnishing a 98.2% conversion of CAL with 93.9% selectivity toward COL (Table 2, entry 5). When Pt nanoparticles were supported on $CoAl_2O_4$ SCMOs, the $Pt/CoAl_2O_4$ catalyst furnished nearly complete CAL conversion

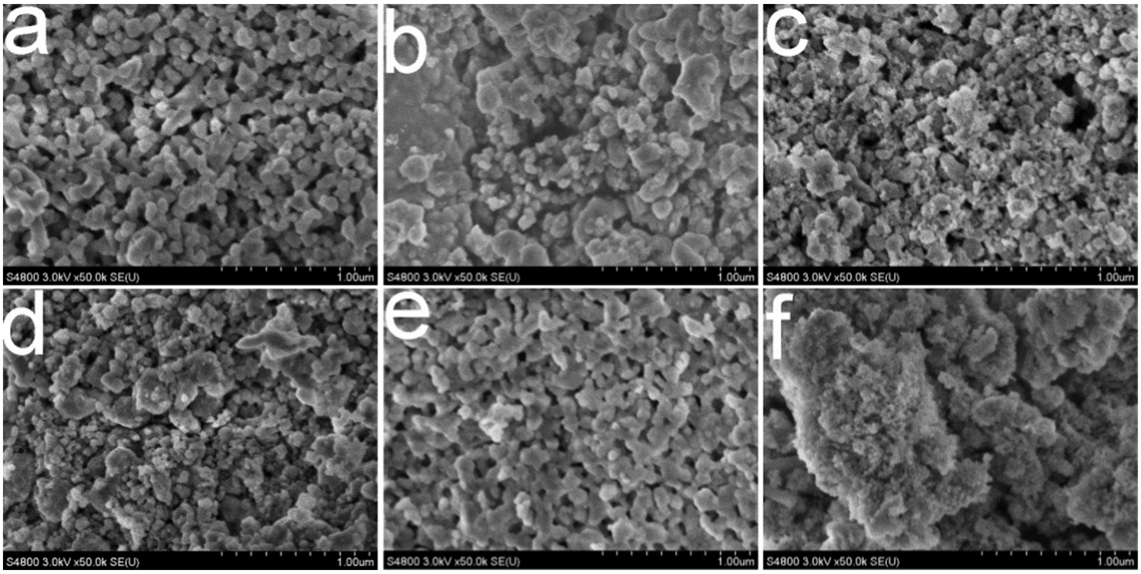

Fig. 3. SEM images of (a) $Pt/FeAl_2O_{4+\delta}$, (b) $Pt/Co_{0.3}Fe_{0.7}Al_2O_{4+\delta}$, (c) $Pt/Co_{0.5}Fe_{0.5}Al_2O_{4+\delta}$, (d) $Pt/Co_{0.7}Fe_{0.3}Al_2O_{4+\delta}$, (e) $Pt/CoAl_2O_4$ and (f) used $Pt/Co_{0.5}Fe_{0.5}Al_2O_{4+\delta}$ after ten runs.

Please cite this article as: H. Xin, Y. Xue, W. Zhang et al., $Co_xFe_{1-x}Al_2O_{4+\delta}$ composite oxides supported Pt nanoparticles as efficient and recyclable catalysts for the liquid-phase selective hydrogenation of cinnamaldehyde, Journal of Catalysis, https://doi.org/10.1016/j.jcat.2019.09.042

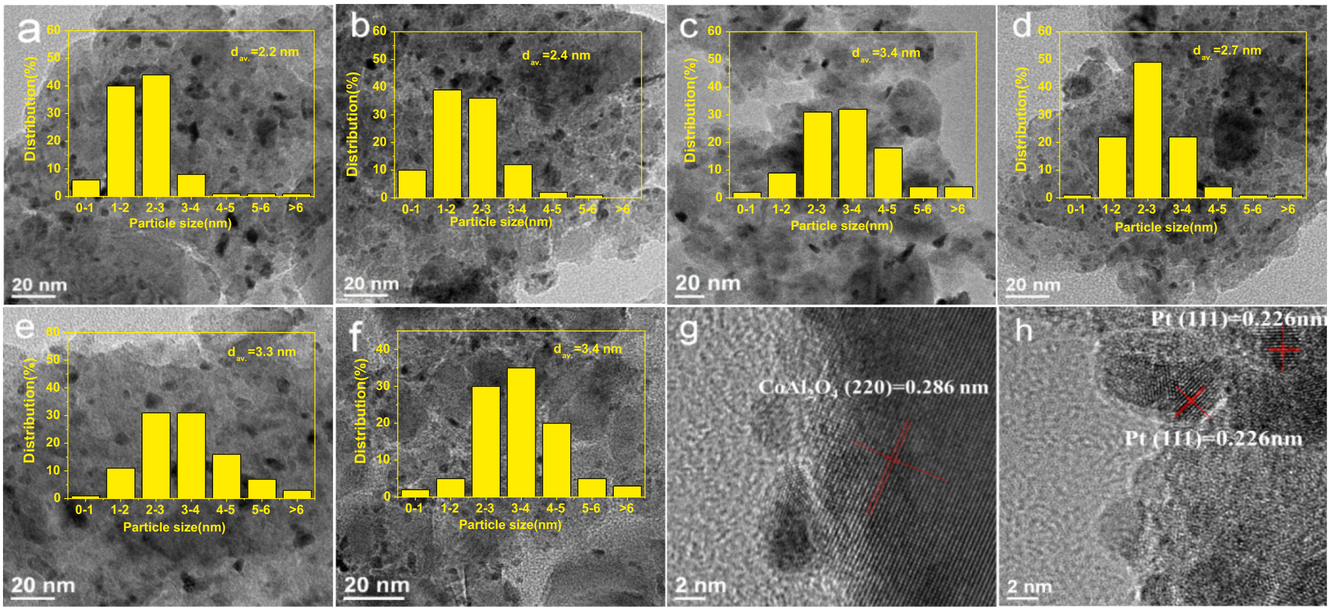

Fig. 4. TEM images and particle size distributions of (a) $Pt/FeAl_2O_{4+\delta}$, (b) $Pt/Co_{0.3}Fe_{0.7}Al_2O_{4+\delta}$, (c) $Pt/Co_{0.5}Fe_{0.5}Al_2O_{4+\delta}$, (d) $Pt/Co_{0.7}Fe_{0.3}Al_2O_{4+\delta}$, (e) $Pt/CoAl_2O_4$ and (f) used $Pt/Co_{0.5}Fe_{0.5}Al_2O_{4+\delta}$ after 10 cycles, and the HRTEM images of (g) $CoAl_2O_4$ and (h) $Pt/FeAl_2O_{4+\delta}$.

Table 2
Hydrogenation of CAL with different Pt-based catalysts [a.]

Entry	Catalyst	Conv. (%)	MSA_{CAL} [b] ($mol\cdot g_{Pt}^{-1}\cdot h^{-1}$)	Sel. (%)		
				COL	HCAL	HCOL
1	$Co_{0.5}Fe_{0.5}Al_2O_{4+\delta}$	2.8	–	87.2	12.8	0
2	$Pt/FeAl_2O_{4+\delta}$	78.6	6.2	90.8	5.8	3.4
3	$Pt/Co_{0.3}Fe_{0.7}Al_2O_{4+\delta}$	90.3	5.9	94.3	2.4	3.3
4	$Pt/Co_{0.5}Fe_{0.5}Al_2O_{4+\delta}$	94.2	7.9	95.0	1.1	3.9
5	$Pt/Co_{0.7}Fe_{0.3}Al_2O_{4+\delta}$	98.2	7.8	93.9	0.8	5.3
6	$Pt/CoAl_2O_4$	99.4	7.3	82.3	0.1	17.6
7	$Pt/Co_{0.5}Fe_{0.5}Al_2O_{4+\delta}$ [c]	71.4	–	94.7	2.9	2.4
8	$Pt-Co_{0.25}/FeAl_2O_{4+\delta}$ [d]	60.1	–	94.3	3.7	2.0
9	$Pt-Fe_{0.25}/CoAl_2O_4$ [d]	85.2	–	93.4	3.2	3.4

[a] Reaction conditions: 25 mg Pt catalyst; 0.5 g CAL; 2.0 MPa H_2; 9 mL isopropyl alcohol +1 mL water; 1200 rpm; 363 K; 0.5 h.
[b] MSR (mass specific rate) was defined as the converted CAL moles per gram of Pt per hour.
[c] The $Co_{0.5}Fe_{0.5}Al_2O_{4+\delta}$ without using glucose as a template was used for loading Pt nanoparticles.
[d] Co or Fe was impregnated with the Pt precursor on $FeAl_2O_{4+\delta}$ or $CoAl_2O_4$ and the molar ratio of Co or Fe to Pt is 0.25.

under the same conditions, although a lower COL selectivity of 82.3% was obtained instead, which might be caused by the consecutive hydrogenation of COL to HCOL, because the HCOL selectivity (17.6%) was obviously higher than the others (Table 2, entry 6). The mass specific rate (MSR, defined as the converted CAL moles per gram of Pt per hour) was also calculated and listed in Table 2. Correspondingly, an MSR of 5.9–7.9 $mol\cdot g_{Pt}^{-1}\cdot h^{-1}$ was achieved with different $Pt/Co_xFe_{1-x}Al_2O_{4+\delta}$ catalysts.

Furthermore, in order to verify the porous effect of $Co_xFe_{1-x}Al_2O_{4+\delta}$ SCMOs prepared using glucose as template, the $Co_{0.5}Fe_{0.5}Al_2O_{4+\delta}$ analogue prepared without using glucose as template was applied to load Pt nanoparticles as well. To our disappointment, only 71.4% CAL conversion was obtained, much lower than its analogue (to compare entries 4 and 7), although the COL selectivity was comparable, indicating that the porous structure of the $Co_xFe_{1-x}Al_2O_{4+\delta}$ SCMOs prepared using glucose as template is indeed beneficial for the mass transfer of the liquid-phase selective hydrogenation of CAL (Table 2, entry 7). In addition, to compare the contact effect of Pt with Fe or Co species on the selective hydrogenation of CAL, we also prepared $Pt-Fe(Co)/Co(Fe)Al_2O_{4+\delta}$ catalysts with a Fe(Co)/Pt molar ratio of 0.25 by co-impregnating Pt precursor and Fe (or Co) precursor simultaneously on $CoAl_2O_4$ (or $FeAl_2O_{4+\delta}$) SCMOs. Although the COL selectivity obtained over $Pt-Fe_{0.25}/CoAl_2O_4$ or $Pt-Co_{0.25}/FeAl_2O_{4+\delta}$ was slightly improved, the CAL conversions were remarkably decreased when compared with $Pt/CoAl_2O_4$ and $Pt/FeAl_2O_{4+\delta}$ under the same conditions. As a result, the CAL conversion decreased from 78.6% with $Pt/FeAl_2O_{4+\delta}$ to 60.1% with $Pt-Co_{0.25}/FeAl_2O_{4+\delta}$; while the CAL conversion decreased from 99.4% with $Pt/CoAl_2O_4$ to 85.2% with $Pt-Fe_{0.25}/CoAl_2O_4$ (Table 2, entries 8 and 9). This implies that after adding Fe (or Co) to $Pt/CoAl_2O_4$ (or $Pt/FeAl_2O_{4+\delta}$), the overall catalytic performance was decreased instead, probably due to coverage of Pt active sites by Fe (or Co) species without good dispersion.

Moreover, although the catalyst was washed with plenty of deionized water to remove Na ions after reduced in an aqueous solution of sodium formate, we cannot guarantee there are no Na ions residues on the catalyst surface. To make clear whether the residual sodium ions have an influence on the reaction results, we added sodium formate with different amount to the reaction system. As listed in Table S1 in the Supporting Information, CAL conversion decreased obviously with increase of the sodium formate while COL selectivity slightly decreased, suggesting the

Please cite this article as: H. Xin, Y. Xue, W. Zhang et al., $Co_xFe_{1-x}Al_2O_{4+\delta}$ composite oxides supported Pt nanoparticles as efficient and recyclable catalysts for the liquid-phase selective hydrogenation of cinnamaldehyde, Journal of Catalysis, https://doi.org/10.1016/j.jcat.2019.09.042

negative influence of sodium ions on this reaction. With regards of extra non-structural Co ions, they indeed can also polarize the C=O bond of CAL.

When compared the results obtained for the selective hydrogenation of CAL with different Pt/$Co_xFe_{1-x}Al_2O_{4+\delta}$ catalysts, CAL conversion increased with the Co/(Fe + Co) molar ratio from 78.6% to 99.4% when *x* increased from 0 to 1. However, the selectivity toward COL almost remained a steady state in the range of 90.8–95.0% and the highest value was obtained with the Pt/$Co_{0.5}Fe_{0.5}Al_2O_{4+\delta}$ catalyst, with an exception encountered for the Pt/$CoAl_2O_4$ catalyst. Therefore, we chose the Pt/$Co_{0.5}Fe_{0.5}Al_2O_{4+\delta}$ as a model catalyst for the further investigations.

To understand the evolution of the hydrogenation products, we investigated the kinetic behaviors of the selective hydrogenation of CAL with the Pt/$Co_{0.5}Fe_{0.5}Al_2O_{4+\delta}$ catalyst at different temperatures. As shown in Fig. 5A, the CAL conversion increased smoothly with reaction time at whatever temperatures and obviously, for the reaction performed at 363 K, the CAL conversion increased faster than those at 333 K and at RT. Nevertheless, the COL selectivity almost kept the same level of around 95% till full conversion of CAL (Fig. 5B). Due to the sequential hydrogenation of COL to HCOL, the selectivity toward COL slightly decreased; while the HCOL selectivity increased rapidly after CAL was exhausted. With regards of the selectivity toward HCAL, it is always as low as 5%. According to the kinetic behaviors at different temperatures, we drew $\ln(C_0/C_t)$ (where C_0 represents the initial molar concentration of CAL; while C_t represents the molar concentration of CAL varied with reaction time) *vs* time curves in Fig. 5C. The linear correlation definitely showed that the selective hydrogenation of CAL on the Pt/$Co_{0.5}Fe_{0.5}Al_2O_{4+\delta}$ catalyst was the first order reaction with respect of CAL. The reaction rate constant *k* obtained at 363 K (0.0977 min^{-1}) was higher than that obtained at 333 K (0.0561 min^{-1}) or at RT (0.0243 min^{-1}). The apparent activation energy *Ea* (21.3 $kJ\cdot mol^{-1}$) was also calculated according to Arrhenius equation (Fig. 5D). Furthermore, we also calculated the initial activity (in terms of TOF, defined as the converted CAL molecules per mole of surface Pt atoms per second) according to the CAL conversions within 5 min and the TOF reached 4.1 s^{-1} over the Pt/$Co_{0.5}Fe_{0.5}Al_2O_{4+\delta}$ catalyst at 363 K, furnishing an initial MSR of 24.5 $mol_{CAL}\cdot g_{Pt}^{-1}\cdot h^{-1}$.

For heterogeneous catalysts involved in a liquid-phase reaction, one of the important issue is to verify their stability and reusability. Hence, the recyclability of the Pt/$Co_{0.5}Fe_{0.5}Al_2O_{4+\delta}$ catalyst towards the liquid-phase selective hydrogenation of CAL was also investigated. Consequently, the Pt/$Co_{0.5}Fe_{0.5}Al_2O_{4+\delta}$ catalyst can be recycled for at least 10 times and only slight loss in CAL conversion was observed. As for the COL selectivity, it showed no distinct loss even after ten cycles and almost kept above 95% (Fig. 6A). To check the catalyst stability, the Pt leaching amount in the filtrate was detected using ICP-AES. To our delight, the amount of the

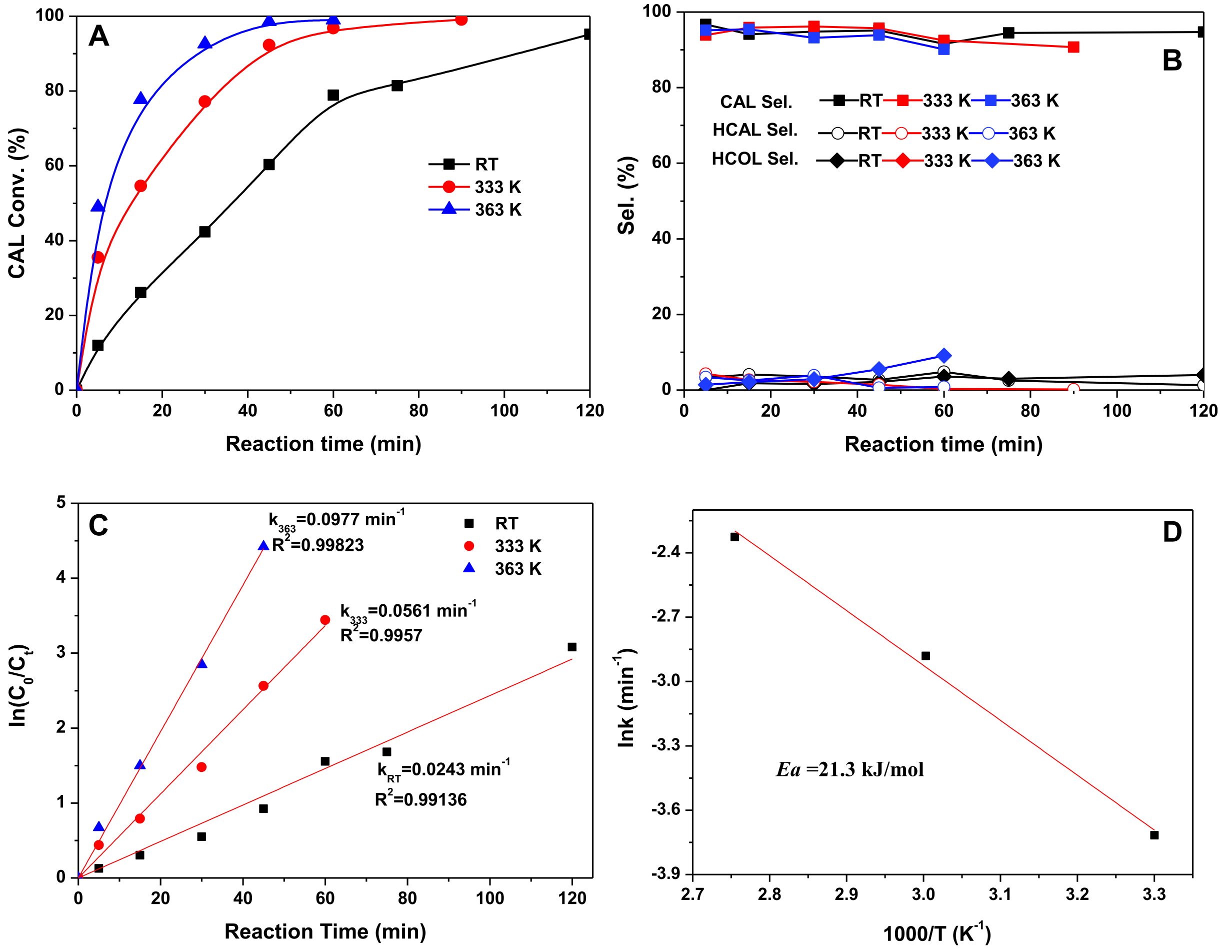

Fig. 5. (A) CAL conversion and (B) selectivity *vs* reaction time curves towards the liquid-phase selective hydrogenation of CAL with Pt/$Co_{0.5}Fe_{0.5}Al_2O_{4+\delta}$ at RT, 333 K and 363 K, respectively. (C) $\ln C_0/C_t$ *vs* time curves at different temperatures, where C_0 represents the initial molar concentration of CAL while C_t represents the molar concentration of CAL varied with reaction time. (D) Apparent activation energy (*Ea*) for the selective hydrogenation of CAL on the Pt/$Co_{0.5}Fe_{0.5}Al_2O_{4+\delta}$ catalyst. Reaction conditions: 25 mg Pt/$Co_{0.5}Fe_{0.5}Al_2O_{4+\delta}$ catalyst; 0.5 g CAL; 2.0 MPa; 9 mL isopropyl alcohol + 1 mL water; 1200 rpm.

Please cite this article as: H. Xin, Y. Xue, W. Zhang et al., $Co_xFe_{1-x}Al_2O_{4+\delta}$ composite oxides supported Pt nanoparticles as efficient and recyclable catalysts for the liquid-phase selective hydrogenation of cinnamaldehyde, Journal of Catalysis, https://doi.org/10.1016/j.jcat.2019.09.042

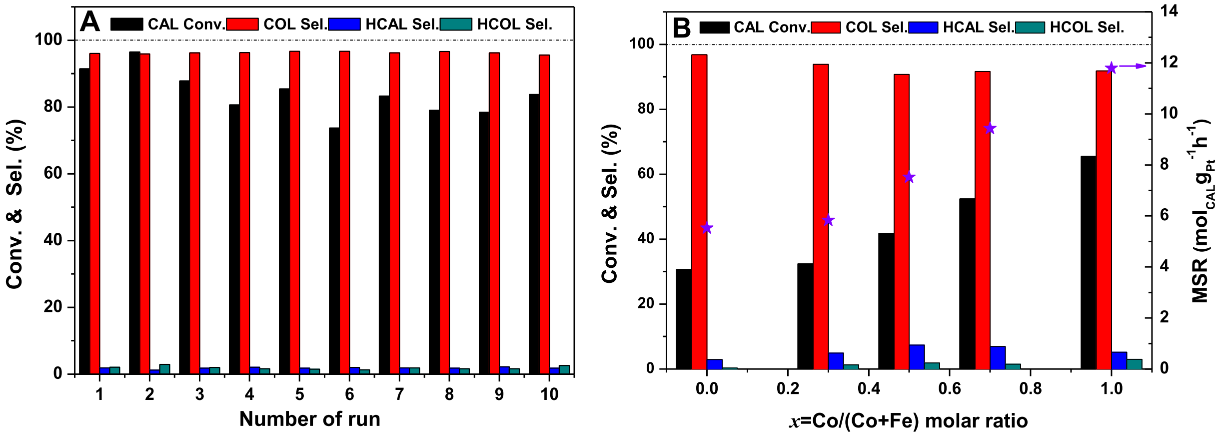

Fig. 6. (A) Recycling of the Pt/$Co_{0.5}Fe_{0.5}Al_2O_{4+\delta}$ catalyst in the liquid-phase selective hydrogenation of CAL at 363 K. Reaction conditions are identical to Table 2. (B) Hydrogenation of CAL with different Pt/$Co_xFe_{1-x}Al_2O_{4+\delta}$ catalysts. Reaction conditions are identical to Table 2 except for 1.5 g CAL.

leached Pt was below the detection limit of ICP-AES. Furthermore, the used Pt/$Co_{0.5}Fe_{0.5}Al_2O_{4+\delta}$ catalyst was also characterized in detail. The TEM image displayed in Fig. 4f shows that the Pt nanoparticles hardly aggregated after ten cycles and the Pt particle size distribution of the used Pt/$Co_{0.5}Fe_{0.5}Al_2O_{4+\delta}$ is centered at 3.4 nm, comparable with the fresh one. The morphology of the used Pt/$Co_{0.5}Fe_{0.5}Al_2O_{4+\delta}$ catalyst looks a little fluffier than the fresh one (Fig. 3f). As for the slight loss in CAL conversion, it might be caused by catalyst loss. We weighed the recovered catalyst after ten cycles, as a result, only a half of the fresh catalyst was retained. This indicates that about half of the submitted catalyst was washed off from the catalytic system during 10 reaction runs, which may be the key reason for the decreased CAL conversion during the recycling processes.

Moreover, to explore the superior catalytic performance of the Pt/$Co_xFe_{1-x}Al_2O_{4+\delta}$ catalysts to the greatest extent, the substrate/catalyst molar ratio was increased to three times with the same catalyst dosage. The correlation between CAL conversion or COL selectivity and Co/(Co + Fe) molar ratio (x value) was also made (Fig. 6B). It is found the conversion of CAL increased obviously with the x value from 0 to 1. However, the selectivity to the desired COL only slightly declined from 94.8% to 91.8% with the x value. Correspondingly, the Pt/$CoAl_2O_4$ catalyst showed a 65.5% CAL conversion, reaching an average MSR of 14.4 $mol_{CAL}\cdot g_{Pt}^{-1}\cdot h^{-1}$, about twice of that obtained with the same catalyst performed at a lower substrate/catalyst molar ratio.

Additionally, in order to further understand the Pt/$Co_xFe_{1-x}Al_2O_{4+\delta}$ catalysts, we compared the Pt/$Co_xFe_{1-x}Al_2O_{4+\delta}$ catalysts with other Pt-based catalysts reported in the literature for the selective hydrogenation of CAL. Table 3 summarizes the detailed comparison results. Clearly, the catalytic performance of the Pt-based catalysts for the selective hydrogenation of CAL was greatly affected by several factors, such as support materials, the second metal component and reaction parameters. By comparison with different materials (such as n-Al_2O_3 [35], SiC-C [36], $CeZrO_2$-1.5 [37], ZnFe-LDH [38], AlCo-MMO [14], FeFe-LDH [16], and $YCo_{0.3}Fe_{0.7}O_3$ perovskite composites [15]) supported monometallic Pt catalysts, 1D PtFe metal nanowires [17] and the second metal-promoted Pt catalysts (including $PtFe_{0.25}$/15AS [9], $PtFe_{0.25}$/15TS [10], Pt-Mo_2N/SBA-15 [39], Pt_3Fe/CNT [40], $Pt_3Co@Co(OH)_2$ [41], even Co-MOF-74@(Pt@Fe_2O_3) [42]), the Pt/$Co_{0.5}Fe_{0.5}Al_2O_{4+\delta}$ catalyst in this work furnished better results, in particular for activity (in terms of either TOF or MSR). Under the similar reaction conditions, the Pt/$Co_{0.5}Fe_{0.5}Al_2O_{4+\delta}$ catalyst showed higher TOF values than most of the Pt-based catalysts, such as $PtFe_{0.25}$/15AS, $PtFe_{0.25}$/15TS, Pt-Mo_2N/SBA-15 and Pt/FeFe-LDH. Of particular note is that the catalytic activity of the Pt/$Co_{0.5}Fe_{0.5}Al_2O_{4+\delta}$ catalyst is comparable with that obtained over the Pt catalyst supported on $YCo_{0.3}Fe_{0.7}O_3$ perovskite composites, which also bears uniformly dispersed Fe and Co species and would have intimate contact with Pt nanoparticles. With regards of the selectivity to the desired product COL furnished by the Pt/$Co_{0.5}Fe_{0.5}Al_2O_{4+\delta}$ catalyst, it is also one of the best values

Table 3
Comparison of the Pt-based catalysts for the selective hydrogenation of CAL to yield COL.

Catalyst	T (K)	P_{H2} (MPa)	t (h)	Conv. (%)	COL Sel. (%)	TOF (h^{-1})	MSR [a] ($mol\cdot g_{Pt}^{-1}\cdot h^{-1}$)	Ref.
Pt-1a/n-Al_2O_3	303	1.0	3	99.0	91.0	3746	–	35
$PtFe_{0.25}$/15AS	363	2.0	1	77.4	76.9	5544	13.9	9
$PtFe_{0.25}$/15TS	363	2.0	0.5	68.0	86.4	11,016	12.2	10
Pt/SiC-C	298	2.0	1	84.9	80.0	2446	–	36
Pt/$YCo_{0.3}Fe_{0.7}O_3$	363	2.0	0.5	98.9	94.9	15,163	31.1	15
Pt/$CeZrO_2$-1.5	333	1.0	0.5	95.0	94.0	10,423	–	37
Pt-Mo_2N/SBA-15	353	1.0	2	70.8	76.9	521	–	39
Pt/ZnFe-LDH	333	2.0	2.0	95.2	91.0	–	2.5	38
Pt/AlCo-MMO	343	2.0	2.0	93.1	75.9	–	3.9	14
Pt/FeFe-LDH	383	1.0	2.0	90.0	92.0	1026	–	16
PtFe NWs	343	0.1	2.5	95.7	95.5	100	–	17
Pt_3Fe/CNT	333	2.0	0.5	62.1	97.2	1200	–	40
$Pt_3Co@Co(OH)_2$	343	0.5	2.0	99.6	90.3	40.9	–	41
Co-MOF-74@(Pt@Fe_2O_3)	RT	1.0	1.0	63.0	100.0	245.7		42
Pt/$Co_{0.5}Fe_{0.5}Al_2O_{4+\delta}$	363	2.0	0.5	94.2	95.0	14,753	24.5	This work

[a] MSR (mass specific rate) was defined as the converted CAL moles per gram of Pt per hour.

Please cite this article as: H. Xin, Y. Xue, W. Zhang et al., $Co_xFe_{1-x}Al_2O_{4+\delta}$ composite oxides supported Pt nanoparticles as efficient and recyclable catalysts for the liquid-phase selective hydrogenation of cinnamaldehyde, Journal of Catalysis, https://doi.org/10.1016/j.jcat.2019.09.042

among all of the Pt-based catalysts reported in the literature up to now.

3.3. Further characterization of the Pt/$Co_xFe_{1-x}Al_2O_{4+\delta}$ catalysts

In order to understand the superiority of the Pt/$Co_xFe_{1-x}Al_2O_{4+\delta}$ catalysts, some representative catalysts were further characterized using a series of techniques. Firstly, the reduction behaviors of as-calcined Pt/$Co_xFe_{1-x}Al_2O_{4+\delta}$ were studied using H_2-TPR technique (Fig. 7A). For as-calcined Pt/$FeAl_2O_{4+\delta}$, there are three reduction peaks, centered at 430, 629 and 868 K, respectively. The sharp peak at 430 K is assigned to reduction of isolated PtO_x [43]. The latter two peaks are attributed to reduction of Fe^{3+} to Fe^0, including two steps, Fe^{3+} to Fe^{2+} (570–670 K) and Fe^{2+} to Fe^0 (750–950 K) [44]. After adding a little Co with the Co/(Fe + Co) molar ratio of 0.3, the reduction peak of PtO_x shifted to 425 K, slightly lower than that for Pt/$FeAl_2O_{4+\delta}$. Correspondingly, the reduction peaks ascribed to the reduction of Fe^{3+} to Fe^0 were also shifted to lower temperatures. With further increasing the x value in the $Co_xFe_{1-x}Al_2O_{4+\delta}$ SCMOs to 0.5, the reduction temperature for PtO_x further decreased; while the reduction of FeO_x disappeared, indicating that the interaction between CoO_x and FeO_x is getting stronger and stronger to form spinel structure in $Co_{0.5}Fe_{0.5}Al_2O_{4+\delta}$ SCMOs. When x value reaches 0.7, the hydrogen uptake split into two peaks, centered at 407 K and 431 K, respectively, which can be ascribed to reduction of PtO_x species with different interaction with $Co_{0.7}Fe_{0.3}Al_2O_{4+\delta}$ SCMOs. If x value further increases to 1, the hydrogen uptake reaches a maximum of 440 K for as-calcined Pt/$CoAl_2O_4$. As for all Co-containing SCMOs, there is also one reduction peak appearing at 1050 K, which can be attributed to the reduction of Co^{2+} to Co^0 [45]. Apparently, among all the as-calcined Pt/$Co_xFe_{1-x}Al_2O_{4+\delta}$ catalysts, the interaction between the Pt and $CoAl_2O_4$ support is the strongest.

Besides H_2-TPR, H_2-TPD analysis was also performed in order to study the hydrogen adsorption ability of different Pt/$Co_xFe_{1-x}Al_2O_{4+\delta}$ catalysts. Previous studies have proved that hydrogen dissociation occurs on the surface of Pt atoms [46], and hydrogen desorption peaks at different temperatures indicate different modes of hydrogen chemisorption. For the Pt/$Co_xFe_{1-x}Al_2O_{4+\delta}$ catalysts in this work, an obvious desorption peak at around 433–443 K is observed, which is attributed to the adsorption of H_2 molecules on Pt atoms. As shown in Fig. 7B, Pt/$Co_xFe_{1-x}Al_2O_{4+\delta}$ shows a relatively increased total integral area of H_2-TPD curves with increase of Co molar ratio and reached a maximum in Pt/$CoAl_2O_4$. As already discussed in H_2-TPR section, the interaction of Pt and $Co_xFe_{1-x}Al_2O_{4+\delta}$ SCMOs would increase the reduction efficiency of Pt, which is then beneficial to hydrogen adsorption. This is consistent with the catalytic performance that the highest results were afforded by the Pt/$CoAl_2O_4$ catalyst.

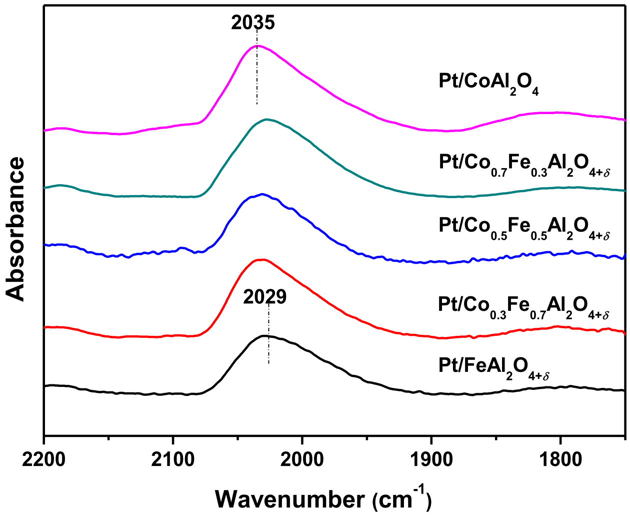

Fig. 8. Infrared spectra of the CO adsorbed on the Pt/$Co_xFe_{1-x}Al_2O_{4+\delta}$ catalysts.

In addition, the acidity of the Pt/$Co_xFe_{1-x}Al_2O_{4+\delta}$ catalysts was determined by NH_3-TPD technique (Fig. 7C). An ammonia desorption peak centered at 500 K was detected for Pt/$FeAl_2O_{4+\delta}$ with the total acid amount of 417.73 μmol·g^{-1}. After adding Co to $Co_xFe_{1-x}Al_2O_{4+\delta}$ SCMOs, the signal for desorbed NH_3 is gradually weakened. With regards of NH_3 desorbed from Pt/$CoAl_2O_4$, it is negligible, demonstrating that the acidity of Pt/$CoAl_2O_4$ is extremely weak. Addition of Co to $FeAl_2O_{4+\delta}$ SCMOs not only changed the SCMOs structure, but also weakened the acidic properties of

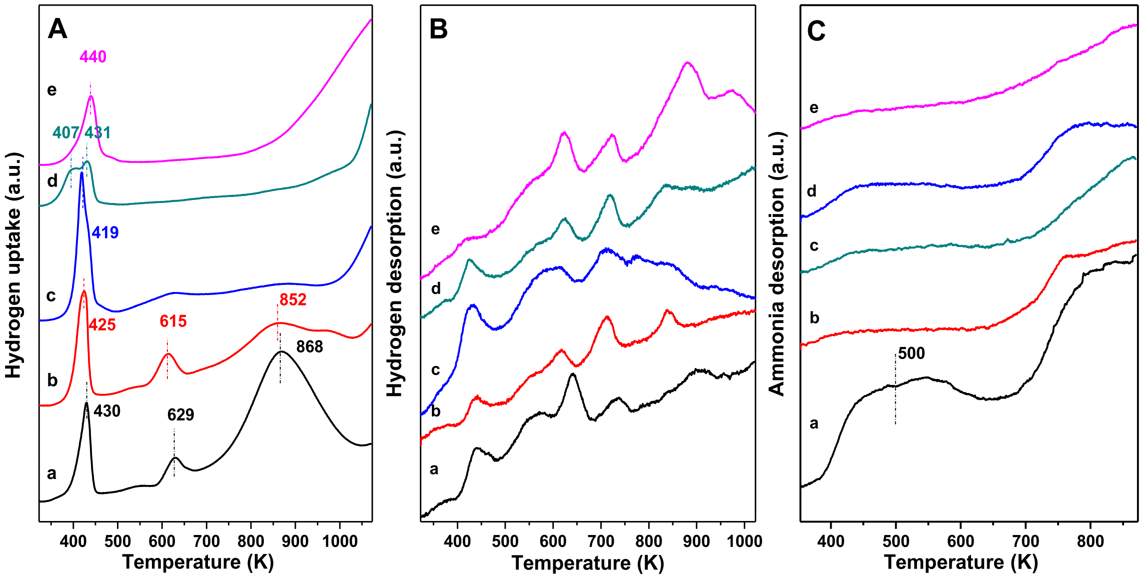

Fig. 7. (A) Temperature-programmed reduction with hydrogen (H_2-TPR) curves, (B) Temperature-programmed desorption of hydrogen (H_2-TPD) curves and (C) Temperature-programmed desorption of ammonia (NH_3-TPD) curves of the (a) Pt/$FeAl_2O_{4+\delta}$, (b) Pt/$Co_{0.3}Fe_{0.7}Al_2O_{4+\delta}$, (c) Pt/$Co_{0.5}Fe_{0.5}Al_2O_{4+\delta}$, (d) Pt/$Co_{0.7}Fe_{0.3}Al_2O_{4+\delta}$, (e) Pt/$CoAl_2O_4$.

Please cite this article as: H. Xin, Y. Xue, W. Zhang et al., $Co_xFe_{1-x}Al_2O_{4+\delta}$ composite oxides supported Pt nanoparticles as efficient and recyclable catalysts for the liquid-phase selective hydrogenation of cinnamaldehyde, Journal of Catalysis, https://doi.org/10.1016/j.jcat.2019.09.042

$FeAl_2O_{4+\delta}$. As a result, the weaker acidity of $Co_xFe_{1\text{-}x}Al_2O_{4+\delta}$ gave rise to larger Pt particle size because the acidity in $FeAl_2O_{4+\delta}$ is helpful for the dispersion of Pt nanoparticles. Therefore, the Pt/$FeAl_2O_{4+\delta}$ catalyst has the smallest Pt particle size. When compared with Pt/$FeAl_2O_{4+\delta}$ with a comparatively larger amount of acidity, Pt/$Co_xFe_{1\text{-}x}Al_2O_{4+\delta}$ ($x \neq 0$) is more effective, suggesting that strong acidity is detrimental for the liquid-phase selective hydrogenation of CAL.

To study the electronic states of Pt, some representative catalysts were further characterized by FT-IR spectroscopy using CO as probe molecules, which is usually used to gain insight into electronic properties. To allow a direct comparison of those data with catalytic results, the Pt/$Co_xFe_{1\text{-}x}Al_2O_{4+\delta}$ catalysts were pretreated in a hydrogen flow at 473 K for 2 h before IR measurements. As shown in Fig. 8, there is an asymmetric CO vibration band in the range of 2100–2000 cm^{-1}, which is ascribed to CO linearly bound to a single Pt atom. As clearly seen in Fig. 8, there is only a tiny red-shift for the linear CO adsorption from 2035 cm^{-1} on Pt/$CoAl_2O_4$ to 2029 cm^{-1} on Pt/$FeAl_2O_{4+\delta}$. When correlating the CO-IR vibration band with the geometry of Pt/$Co_xFe_{1\text{-}x}Al_2O_{4+\delta}$, the CO vibration band at 2029–2035 cm^{-1} can be attributed to linear CO adsorption on low coordinated Pt sites, such as steps, edges, corners, and defect sites [47,48]. Considering that the five Pt/$Co_xFe_{1\text{-}x}Al_2O_{4+\delta}$ catalysts have similar Pt particle sizes of 2.2–3.4 nm, the tiny influence of Pt particle size on the CO vibration band can be neglected. Thus, the lower CO vibration position reflects that the catalyst has higher electron density on Pt atoms, because an increase in the electron density on Pt atoms in turn increases the d-π back donation. This implies that Pt/$FeAl_2O_{4+\delta}$ has higher electron density than Pt/$CoAl_2O_4$, which is well consistent with the H_2-TPR results. Such relatively electron-deficient Pt species of Pt/$CoAl_2O_4$ easily interact with the oxygen atom of carbonyl groups in CAL.

To further characterize the surface electronic properties, the Pt/$Co_xFe_{1\text{-}x}Al_2O_{4+\delta}$ catalysts were probed by XPS after *in situ* pretreated in a hydrogen flow at 473 K for 2 h. The asymmetric peak

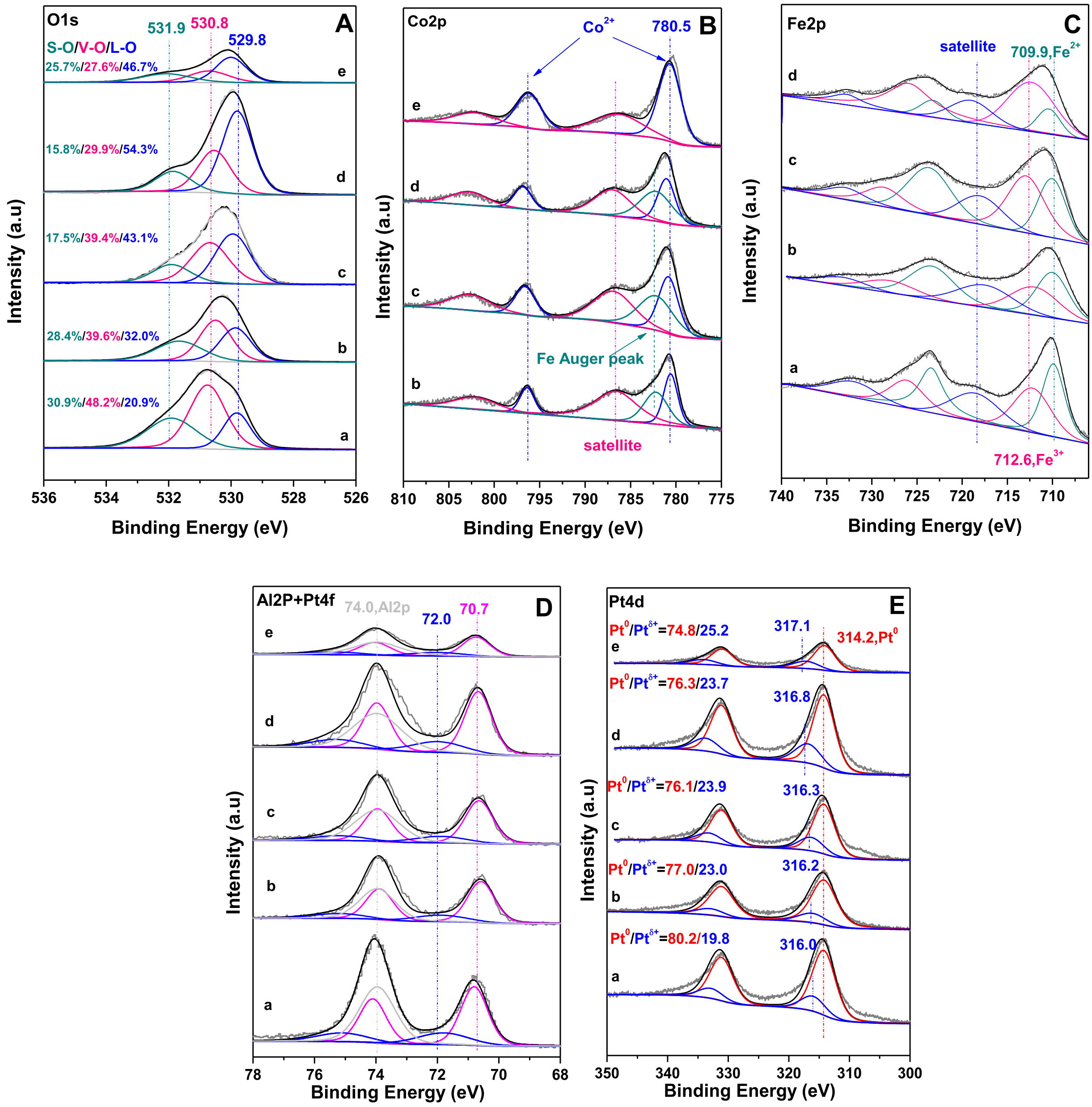

Fig. 9. XPS spectra of (A) O1s, (B) Co2p, (C) Fe2p, (D) Al2p + Pt4f and (E) Pt4d for (a) Pt/$FeAl_2O_{4+\delta}$, (b) Pt/$Co_{0.3}Fe_{0.7}Al_2O_{4+\delta}$, (c) Pt/$Co_{0.5}Fe_{0.5}Al_2O_{4+\delta}$, (d) Pt/$Co_{0.7}Fe_{0.3}Al_2O_{4+\delta}$ and (e) Pt/$CoAl_2O_4$.

Please cite this article as: H. Xin, Y. Xue, W. Zhang et al., $Co_xFe_{1\text{-}x}Al_2O_{4+\delta}$ composite oxides supported Pt nanoparticles as efficient and recyclable catalysts for the liquid-phase selective hydrogenation of cinnamaldehyde, Journal of Catalysis, https://doi.org/10.1016/j.jcat.2019.09.042

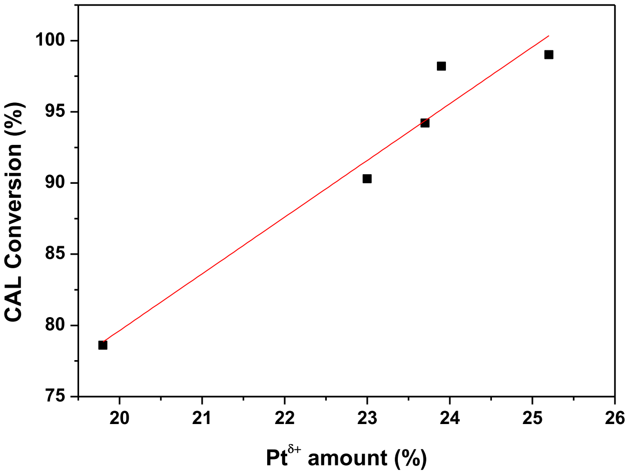

Fig. 10. The correlation of CAL Conversion versus $Pt^{\delta+}$ amount on the Pt/$Co_xFe_{1-x}Al_2O_{4+\delta}$ catalyst according to XPS results.

of O1s could be deconvoluted to three peaks. For Pt/$FeAl_2O_{4+\delta}$, the main peak at BE of 530.8 eV can be assigned to the oxygen vacancy (V—O), while the other two peaks at 529.8 eV and 531.9 eV can be attributed to lattice oxygen (L—O) and surface oxygen (S—O), respectively (Fig. 9A) [15]. After Co was doped in the $Co_{0.3}Fe_{0.7}Al_2O_{4+\delta}$ composites, the core O1s shifts to lower BEs obviously, implying that the different chemical state of oxygen atoms, and the V—O species are predominant for the samples. With further increasing the Co ratio in the $Co_xFe_{1-x}Al_2O_{4+\delta}$ composites (x = 0.5, 0.7, 1), L—O species became predominant, which can be interpreted by forming spinel structure.

The Co2p spectra (Fig. 9B) show the presence of the $2p_{3/2}$ and $2p_{1/2}$ states. The $Co2p_{3/2}$ peaks for the four samples were found to be at 780.5 ± 0.1 eV, which reveals that Co is totally in the oxidized state in that only Co^{2+} species were detected [14,15]. However, in the $Fe2p_{3/2}$ XPS spectra, BE for Fe^{3+} species was centered at 712.6 eV, accompanied by the Fe^{3+} shake up satellite peaks (716–722 eV). The other peak at about 709.9 eV can be deconvoluted, which can be assigned to Fe^{2+}, and the proportion of Fe^{3+} and Fe^{2+} could change with Fe content in the Pt/$Co_xFe_{1-x}Al_2O_{4+\delta}$ (Fig. 9C) [49]. Regarding the chemical state of Al, the peak centered at 74.0 eV, which is mainly in Al_2O_3 form. From Fig. 9D, the $Pt4f_{7/2}$ peaks observed at 70.7 eV can be assigned to Pt^0. The BE at 72.0 eV is lower than that for $Pt4f_{7/2}$ of Pt^{2+} species, but higher than that for $Pt4f_{7/2}$ of Pt^0 species; therefore, it can be attributed to $Pt4f_{7/2}$ of partially charged $Pt^{\delta+}$ species ($0 < \delta < 2$). Since the BEs of Al2p and Pt4f are overlapped, the Pt4d spectra were taken as well to further distinguish the surface electronic properties of Pt atoms.

As shown in Fig. 9E, the Pt4d peak could be deconvoluted to two species. The $Pt4d_{5/2}$ at BE of 314.2 eV is assigned to metallic Pt^0, while the one at 316.0–317.1 eV could be assigned to positively charged $Pt^{\delta+}$ species ($0 < \delta < 2$), because its BE is lower than that of typical Pt^{2+} (317.3 eV) [50]. Nevertheless, the $Pt^{\delta+}$ amount varies with different supports. For Pt/$CoAl_2O_4$, $Pt^{\delta+}$ amount is the highest among the five Pt catalysts, reaching 25.2%; while it is the lowest on the Pt/$FeAl_2O_{4+\delta}$ catalyst (19.8%).

Based on the above discussion, the $CoAl_2O_4$ composites had the lowest V-O concentration, as revealed by XPS characterization. As well known, the V-O can serve as Lewis acid sites, and thus the electron density of the metal atoms (such as Fe or Co ions) adjacent to V-O would be increased, so that the supported Pt species become relatively electron-rich via the interaction of metal-support. This has been proved by the FTIR spectra of CO adsorbed on the Pt/$Co_xFe_{1-x}Al_2O_{4+\delta}$ catalysts. With increasing the Fe amount, the V-O concentration increased and the d-π feedback donation became strong, so that the IR band of linearly-adsorbed CO red-shifted. As also mentioned in the NH_3-TPD characterization, $FeAl_2O_{4+\delta}$ had the highest acidity. As a result, the higher V-O concentration, the higher acidity, the higher content of Pt atoms with the lower content of $Pt^{\delta+}$.

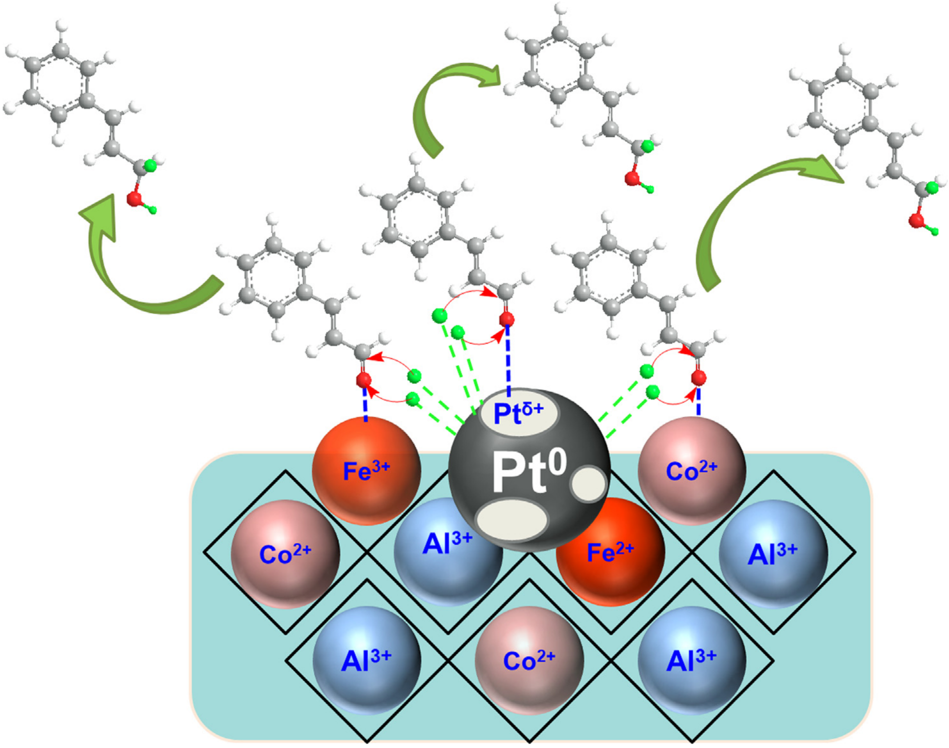

Fig. 11. The hypothesis of CAL adsorption and activation with the Pt/$Co_xFe_{1-x}Al_2O_{4+\delta}$ catalysts.

Please cite this article as: H. Xin, Y. Xue, W. Zhang et al., $Co_xFe_{1-x}Al_2O_{4+\delta}$ composite oxides supported Pt nanoparticles as efficient and recyclable catalysts for the liquid-phase selective hydrogenation of cinnamaldehyde, Journal of Catalysis, https://doi.org/10.1016/j.jcat.2019.09.042

Moreover, in order to better correlate the catalytic results with characterization, we also established a correlation between $Pt^{\delta+}$ amount and the CAL conversion. As a result, there is a positive linear correlation (Fig. 10). In another word, the catalyst with the highest surface $Pt^{\delta+}$ amount furnished the highest CAL conversion. This implies that there are abundant $Pt^{\delta+}$ species on the surface, which can adsorb and activate CAL through the carbonyl group, so that the C═O bond can be preferentially activated and thus hydrogenated to COL. Additionally, the FeO_x and CoO_x species either in SCMOs or in non-structural simple oxides are also helpful for adsorbing and activating the CAL. According to the discussion, the related hypothesis of CAL adsorption and activation with the $Pt/Co_xFe_{1-x}Al_2O_{4+\delta}$ catalysts was also proposed (Fig. 11). Both the positive $Pt^{\delta+}$ species and the FeO_x (or CoO_x) species can adsorb and activate CAL by interaction with oxygen atoms in carbonyl groups, while hydrogen molecules are dissociated on Pt^0 atoms and then transferred to attack the activated CAL to form COL.

4. Conclusion

$Co_xFe_{1-x}Al_2O_{4+\delta}$ spinel composite metal oxides were prepared using a sol-gel method using glucose as template. Although $Co_xFe_{1-x}Al_2O_{4+\delta}$ SCMOs only had 10–20 m^2g^{-1} BET specific surface area, they were proved to be remarkable support for Pt nanoparticles. Pt nanoparticles were uniformly and highly dispersed on the surface of $Co_xFe_{1-x}Al_2O_{4+\delta}$, even the Pt loading reaches about 5 wt% with an average Pt particle size of 2.2–3.4 nm. The $Pt/Co_xFe_{1-x}Al_2O_{4+\delta}$ catalysts showed superior catalytic performance including activity and selectivity for the desired COL. With a Co/(Co + Fe) molar ratio of 0.5, the $Pt/Co_{0.5}Fe_{0.5}Al_2O_{4+\delta}$ catalyst furnished 95% selectivity to COL at 94.2% conversion of CAL, with an initial MSR of 24.5 $mol \cdot g_{Pt}^{-1} \cdot h^{-1}$ and an initial activity of 4.1 s^{-1} TOF. The $Pt/Co_{0.5}Fe_{0.5}Al_2O_{4+\delta}$ catalyst can also be recycled for at least 10 times without distinct loss in activity or selectivity to the desired COL. Combined with the detailed characterization results, we can conclude that the intimate contact of Pt with FeO_x/CoO_x plays an important role in determining the catalytic performance of the $Pt/Co_xFe_{1-x}Al_2O_{4+\delta}$ catalysts. With increase of Co/(Co + Fe) molar ratio, the interaction between Pt and FeO_x (or CoO_x) species becomes stronger and thus the surface $Pt^{\delta+}$ amount increased obviously. Therefore, the Pt species with appropriate positive charges and FeO_x (or CoO_x) species are beneficial for the preferential adsorption and activation of terminal C═O groups. The $Pt/Co_xFe_{1-x}Al_2O_{4+\delta}$ catalysts are also promising catalysts for other hydrogenation reactions.

Acknowledgements

This work was supported by the National Natural Science Foundation of China (Grant No. 21872052 and 21872054).

Appendix A. Supplementary material

Supplementary data to this article can be found online at https://doi.org/10.1016/j.jcat.2019.09.042.

References

[1] W. Yu, Y. Wang, H. Liu, W. Zheng, Preparation and characterization of polymer-protected Pt/Co bimetallic colloids and their catalytic properties in the selective hydrogenation of cinnamaldehyde, J. Mol. Catal. A 112 (1996) 105–113.

[2] K. Sun, Y. Hong, G. Zhang, B. Xu, Synergy between Pt and Au in Pt-on-Au nanostructures for chemoselective hydrogenation catalysis, ACS Catal. 1 (2011) 1336–1346.

[3] S. Chen, L. Meng, B. Chen, W. Chen, X. Duan, X. Huang, B. Zhang, H. Fu, Y. Wan, Poison tolerance to the selective hydrogenation of cinnamaldehyde in water over an ordered mesoporous carbonaceous composite supported Pd catalyst, ACS Catal. 7 (2017) 2074–2087.

[4] P. Bhanja, X. Liu, A. Modak, Pt and Pd nanoparticles immobilized on amine-functionalized hypercrosslinked porous polymer nanotubes as selective hydrogenation catalyst for α,β -unsaturated aldehydes, ChemistrySelect 2 (2017) 7535–7543.

[5] S. Lu, W.W. Lonergan, J.P. Bosco, S. Wang, Y. Zhu, Y. Xie, J.G. Chen, Low temperature hydrogenation of benzene and cyclohexene: A comparative study between γ-Al_2O_3 supported PtCo and PtNi bimetallic catalysts, J. Catal. 259 (2008) 260–268.

[6] Z. Guo, Y. Chen, L. Li, X. Wang, G.L. Haller, Y. Yang, Carbon nanotube-supported Pt-based bimetallic catalysts prepared by a microwave-assisted polyol reduction method and their catalytic applications in the selective hydrogenation, J. Catal. 276 (2010) 314–326.

[7] A.J. Plomp, D.M. van Asten, A.M. van der Eerden, P. Mäki-Arvela, D.Y. Murzin, K.P. Jong, J.H. Bitter, Catalysts based on platinum-tin and platinum-gallium in close contact for the selective hydrogenation of cinnamaldehyde, J. Catal. 263 (2009) 146–154.

[8] L. Chen, H. Chen, Y. Li, One-pot synthesis of Pd@MOF composites without the addition of stabilizing agents, Chem. Commun. 50 (2014) 14752–14755.

[9] H. Pan, J. Li, J. Lu, G. Wang, W. Xie, P. Wu, X. Li, Selective hydrogenation of cinnamaldehyde with $PtFe_x/Al_2O_3$@SBA-15 catalyst: Enhancement in activity and selectivity to unsaturated alcohol by Pt-FeO_x and Pt-Al_2O_3@SBA-15 interaction, J. Catal. 354 (2017) 24–36.

[10] Y. Xue, R. Yao, J. Li, G. Wang, P. Wu, X. Li, Efficient Pt-FeO_x/TiO_2@SBA-15 catalysts for selective hydrogenation of cinnamaldehyde to cinnamyl alcohol, Catal. Sci. Technol. 7 (2017) 6112–6123.

[11] S. Bhogeswararao, D. Srinivas, Intramolecular selective hydrogenation of cinnamaldehyde over CeO_2-ZrO_2 supported Pt catalysts, J. Catal. 285 (2012) 31–40.

[12] Z. Weng, F. Zaera, Sub-monolayer control of mixed-oxide support composition in catalysts via atomic layer deposition: Selective hydrogenation of cinnamaldehyde promoted by (SiO_2-ALD)-Pt/Al_2O_3, ACS Catal. 8 (2018) 8513–8524.

[13] Q. Wu, C. Zhang, B. Zhang, X. Li, Z. Ying, T. Liu, W. Lin, Y. Yu, H. Cheng, F. Zhao, Highly selective Pt/ordered mesoporous TiO_2-SiO_2 catalysts for hydrogenation of cinnamaldehyde: The promoting role of Ti^{2+}, J. Coll. Interf. Sci. 463 (2016) 75–82.

[14] Z. Tian, Q. Li, J. Hou, L. Pei, Y. Li, S. Ai, Platinum nanocrystals supported on CoAl mixed metal oxide nanosheets derived from layered double hydroxides as catalysts for selective hydrogenation of cinnamaldehyde, J. Catal. 331 (2015) 193–202.

[15] Y. Xue, H. Xin, W. Xie, P. Wu, X. Li, Pt nanoparticles supported on $YCo_xFe_{1-x}O_3$ perovskite oxides: highly efficient catalysts for liquid-phase hydrogenation of cinnamaldehyde, Chem. Commun. 55 (2019) 3363–3366.

[16] Y. Zhang, S. Wei, Y. Lin, G. Fan, F. Li, Dispersing metallic platinum on green rust enables effective and selective hydrogenation of carbonyl group in cinnamaldehyde, ACS Omega 3 (2018) 12778–12787.

[17] S. Bai, L. Bu, Q. Shao, X. Zhu, X. Huang, Multicomponent Pt-based zigzag nanowires as selectivity controllers for selective hydrogenation reactions, J. Am. Chem. Soc. 140 (2018) 8384–8387.

[18] M. Zhu, B. Huang, Q. Shao, Y. Pi, Y. Qian, X. Huang, Highly networked platinum-tin nanowires as highly active and selective catalysts towards the semihydrogenation of unsaturated aldehydes, ChemCatChem 10 (2018) 3214–3218.

[19] C. Yang, S. Bai, Y. Feng, X. Huang, An on-demand, selective hydrogenation catalysis over Pt-Fe nanocatalysts under ambient condition, ChemCatChem 11 (2019) 2265–2269.

[20] X. Wang, Y. He, Y. Liu, J. Park, X. Liang, Atomic layer deposited Pt-Co bimetallic catalysts for selective hydrogenation of α,β -unsaturated aldehydes to unsaturated alcohols, J. Catal. 366 (2018) 61–69.

[21] Q. Wang, G. Wang, H. Xin, J. Liu, G. Xiong, P. Wu, X. Li, Sn-doped Pt catalyst supported on hierarchical porous ZSM-5 for the liquid-phase hydrogenation of cinnamaldehyde, Catal. Sci. Technol. 9 (2019) 3226–3237.

[22] K. Yuan, T. Song, D. Wang, X. Zhang, X. Gao, Y. Zou, H. Dong, Z. Tang, W. Hu, Effective and selective catalysts for cinnamaldehyde hydrogenation: Hydrophobic hybrids of metal-organic frameworks, metal nanoparticles, and micro-and mesoporous polymers, Angew. Chem. Int. Ed. 57 (2018) 5708–5713.

[23] L. Chang, Y. Li, One-step encapsulation of Pt-Co bimetallic nanoparticles within MOFs for advanced room temperature nanocatalysis, Mol. Catal. 433 (2017) 77–83.

[24] K.B. Vu, K.V. Bukhryakov, D.H. Anjum, V.O. Rodionov, Surface-bound ligands modulate chemoselectivity and activity of a bimetallic nanoparticle catalyst, ACS Catal. 5 (2015) 2529–2533.

[25] K.R. Kahsar, D.K. Schwartz, J.W. Medlin, Control of metal catalyst selectivity through specific noncovalent molecular interactions, J. Am. Chem. Soc. 136 (2014) 520–526.

[26] K.R. Kahsar, D.K. Schwartz, J.W. Medlin, Stability of self-assembled monolayer coated Pt/Al_2O_3 catalysts for liquid phase hydrogenation, J. Mol. Catal. A 396 (2015) 188–195.

[27] P. Liu, E.J.M. Hensen, Highly efficient and robust Au/$MgCuCr_2O_4$ catalyst for gas-phase oxidation of ethanol to acetaldehyde, J. Am. Chem. Soc. 135 (2013) 14032–14035.

[28] Y. Wang, A. Jia, M. Luo, J. Lu, Highly active spinel type $CoCr_2O_4$ catalysts for dichloromethane oxidation, Appl. Catal. B 165 (2015) 477–486.

Please cite this article as: H. Xin, Y. Xue, W. Zhang et al., $Co_xFe_{1-x}Al_2O_{4+\delta}$ composite oxides supported Pt nanoparticles as efficient and recyclable catalysts for the liquid-phase selective hydrogenation of cinnamaldehyde, Journal of Catalysis, https://doi.org/10.1016/j.jcat.2019.09.042

[29] F. Yan, C. Zhao, L. Yi, J. Zhang, B. Ge, T. Zhang, W. Li, Effect of the degree of dispersion of Pt over $MgAl_2O_4$ on the catalytic hydrogenation of benzaldehyde, Chin. J. Catal. 38 (2017) 1613–1620.

[30] W. Hu, D. Li, Y. Yang, T. Li, H. Chen, P. Liu, Copper ferrite supported gold nanoparticles as efficient and recyclable catalyst for liquid-phase ethanol oxidation, J. Catal. 357 (2018) 108–117.

[31] S.T. Oyama, X. Zhang, J. Lu, Y. Gu, T. Fujitani, Epoxidation of propylene with H_2 and O_2 in the explosive regime in a packed-bed catalytic membrane reactor, J. Catal. 257 (2008) 1–4.

[32] A. Jia, G. Hu, L. Meng, Y. Xie, J. Lu, M. Luo, CO oxidation over $CuO/Ce_{1-x}Cu_xO_{2-\delta}$ and $Ce_{1-x}Cu_xO_{2-\delta}$ catalysts: Synergetic effects and kinetic study, J. Catal. 289 (2012) 199–209.

[33] R.J. Madon, M. Boudart, Experimental criterion for the absence of artifacts in the measurement of rates of heterogeneous catalytic reactions, Ind. Eng. Chem. Fundam. 21 (1982) 438–447.

[34] P. Tarte, Infra-red spectra of inorganic aluminates and characteristic vibrational frequencies of AlO_4 tetrahedra and AlO_6 octahedra, Spectrochim. Acta, Part A 23 (1967) 2127–2143.

[35] H. Liu, Q. Mei, S. Li, Y. Yang, Y. Wang, H. Liu, L. Zheng, P. An, J. Zhang, B. Han, Selective hydrogenation of unsaturated aldehydes over Pt nanoparticles promoted by the cooperation of steric and electronic effects, Chem. Commun. 54 (2018) 908–911.

[36] R. Yao, J. Li, P. Wu, X. Li, The superior performance of a Pt catalyst supported on nanoporous SiC-C composites for liquid-phase selective hydrogenation of cinnamaldehyde, RSC Adv. 6 (2016) 81211–81218.

[37] S. Wei, Y. Zhao, G. Fan, L. Yang, F. Li, Structure-dependent selective hydrogenation of cinnamaldehyde over high-surface-area CeO_2-ZrO_2 composites supported Pt nanoparticles, Chem. Eng. J. 322 (2017) 234–245.

[38] Z. Tian, Q. Li, J. Hou, Y. Li, S. Ai, Highly selective hydrogenation of α, β-unsaturated aldehydes by Pt catalysts supported on Fe-based, Catal. Sci. Technol. 6 (2016) 703–707.

[39] D. Wang, Y. Zhu, C. Tian, L. Wang, W. Zhou, Y. Dong, Q. Han, Y. Liu, F. Yuan, H. Fu, Synergistic effect of Mo_2N and Pt for promoted selective hydrogenation of cinnamaldehyde over Pt-Mo_2N/SBA-15, Catal. Sci. Technol. 6 (2016) 2403–2412.

[40] Y. Dai, X. Gao, X. Chu, C. Jiang, Y. Yao, Z. Guo, C. Zhou, C. Wang, H. Wang, Y. Yang, On the role of water in selective hydrogenation of cinnamaldehyde to cinnamyl alcohol on PtFe catalysts, J. Catal. 364 (2018) 192–203.

[41] H. Wang, S. Bai, Y. Pi, Q. Shao, Y. Tan, X. Huang, A strongly coupled ultrasmall Pt_3Co nanoparticle-ultrathin $Co(OH)_2$ nanosheet architecture enhances selective hydrogenation of α, β-unsaturated aldehydes, ACS Catal. 9 (2019) 154–159.

[42] L. Yang, H. Wu, H. Gao, J. Li, Y. Tao, W. Yin, F. Luo, Hybrid catalyst of a metal-organic framework, metal nanoparticles, and oxide that enables strong steric constraint and metal-support interaction for the highly effective and selective hydrogenation of cinnamaldehyde, Inorg. Chem. 57 (2018) 12461–12465.

[43] N.E. Nunez, H.P. Bideberripe, M. Mizrahi, J.M. Ramallo-Lopez, M.L. Casella, G.J. Siri, CO selective oxidation using co-promoted Pt/γ-Al_2O_3 catalysts, Int. J. Hydrogen Energy 41 (2016) 19005–19013.

[44] A.J.H.M. Kock, H.M. Fortuin, J.W. Geus, The reduction behavior of supported iron catalysts in hydrogen or carbon monoxide atmospheres, J. Catal. 96 (1985) 261–275.

[45] P. Arnoldy, J.A. Moulijn, Temperature-programmed reduction of CoO/Al_2O_3 catalysts, J. Catal. 93 (1985) 38–54.

[46] A.S. Lisitsyn, O.A. Yakovina, On the origin of high-temperature phenomena in Pt/Al_2O_3, Phys. Chem. Chem. Phys. 20 (2018) 2339–2350.

[47] X. Lan, K. Xue, T. Wang, Combined synergetic and steric effects for highly selective hydrogenation of unsaturated aldehyde, J. Catal. 372 (2019) 49–60.

[48] Q. Hu, S. Wang, Z. Gao, Y. Li, Q. Zhang, Q. Xiang, Y. Qin, The precise decoration of Pt nanoparticles with Fe oxide by atomic layer deposition for the selective hydrogenation of cinnamaldehyde, Appl. Catal. B 218 (2017) 591–599.

[49] M. Vijayaraj, C.S. Gopinath, On the "active spacer and stabilizer" role of Zn in $Cu_{1-x}Zn_x$ Fe_2O_4 in the selective mono-N-methylation of aniline: XPS and catalysis study, J. Catal. 241 (2006) 83–95.

[50] G. Corro, C. Cano, J.L.G. Fierro, A study of Pt-Pd/γ-Al_2O_3 catalysts for methane oxidation resistant to deactivation by sulfur poisoning, J. Mol. Catal. A 315 (2010) 35–42.

Please cite this article as: H. Xin, Y. Xue, W. Zhang et al., $Co_xFe_{1-x}Al_2O_{4+\delta}$ composite oxides supported Pt nanoparticles as efficient and recyclable catalysts for the liquid-phase selective hydrogenation of cinnamaldehyde, Journal of Catalysis, https://doi.org/10.1016/j.jcat.2019.09.042